AD-A183 563 OBSERVATIONS OF SHIP WAKES FROM SPACE-SHUTTLE MISSIONS 1/1
(U) ORI INC ARLINGTON VA J M WITTING ET AL. 12 JUN 87
ORI-TR-2727 N00014-86-C-0034

UNCLASSIFIED F/G 20/4 NL

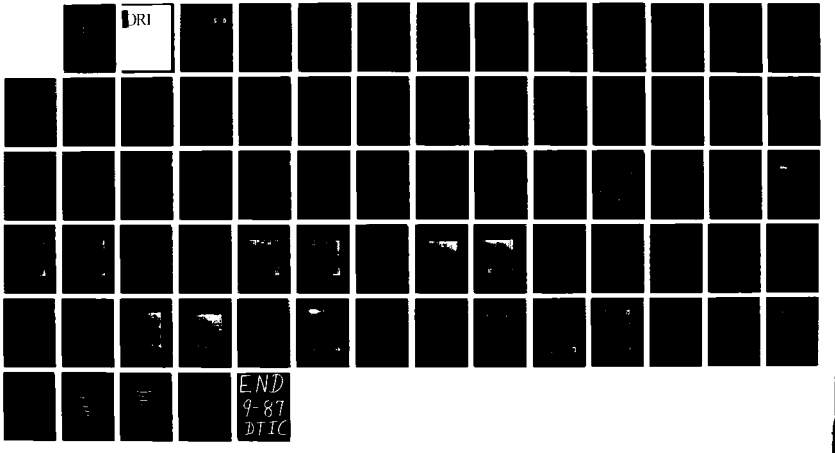

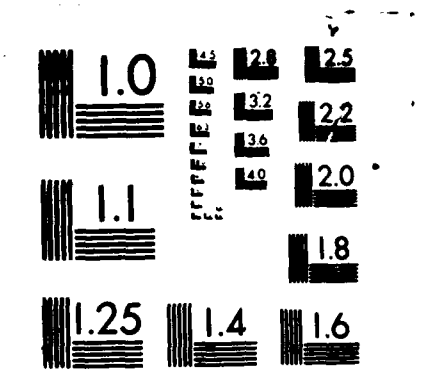

DRI

(12)

TR-2727

ORI 1375 Piccard Drive
Rockville, Maryland 20850

OBSERVATIONS OF SHIP WAKES FROM SPACE-SHUTTLE MISSIONS

TECHNICAL REPORT

12 June 1987

Prepared For:

Office of Naval Research
Department of the Navy
800 North Quincy Street
Arlington, VA 22217-5000

Prepared By:

James M. Witting
Richard F. Hoglund

Contract No. N00014-86-C-0834

Final Report

OBSERVATIONS OF SHIP WAKES FROM SPACE-SHUTTLE MISSIONS

by

James M. Witting & Richard F. Hoglund
ORI, Inc.

1. INTRODUCTION

Highly visible features on the ocean surface behind a moving ship are the Kelvin waves, which appear as a regular pattern moving with the ship, and a ribbon trailing the ship's stern marked by less choppy water than the surrounding, which is produced by the ship's turbulent wake. The Kelvin waves were first described by their namesake (Thomson, 1887), who developed the method of stationary phase to analyze them. The simplest analysis of ship waves that derives a basically correct wave pattern is linear water wave theory with a moving steady source. Figure 1 shows the elevation of the water surface from a simple source moving in a straight line at constant speed [Appendix A outlines a novel computational method that is used to produce the figure; the basic wave pattern is derived and displayed in many books, e.g. Lamb (1932), Stoker (1957), Lighthill (1978), Wehausen & Laitone (1960)]. Waves can exist only in the region between $\pm\sin^{-1}(1/3) = \pm 19.47°$ of the center line. On the edges of the pattern the waves form a cusp; their amplitudes are generally at a maximum just inside the cusp lines. Figure 2, taken from Wehausen & Laitone, shows the geometry locating wave crests. Note that two distinct branches show up, one composed of waves traveling at relatively small angles to the ship direction (the "transverse" pattern), the other composed of waves traveling at relatively large angles to the ship direction (the "divergent" pattern). At the cusp line there is a 90° phase shift between the two patterns, a feature not shown in most authors' corresponding figures [the ordinary method of stationary phase becomes invalid near the cusp; see Ursell (1960) for a more complete treatment that accounts for behavior near the cusp correctly, still, however, valid only at large distances from the ship].

Most people's views of ship waves are visual and are taken from a sea-level vantage point, i.e. they are standing on the ship making the waves and are looking back, or are looking at (other) ships from their own or from the shore. From such a viewpoint the most striking features are the smooth water directly behind the ship and the large-

amplitude waves near the Kelvin-wave cusps. The wide variety of ship-wake morphologies that appeared in the synthetic aperture radar (SAR) imagery from SEASAT, which operated during the summer of 1978, thus surprised the scientific community. A most unforeseen morphology was that of the narrow-V wake, which showed a V-shaped pair of straight lines that intersected at angles the order of a few degrees, rather than the 39° marking the Kelvin-wave cusps. Navy and other federal agencies began programs in the early 1980's to identify the physical mechanisms that are responsible for the variety of SAR imageries of ship wakes, and such programs continue today. The Office of Naval Technology has begun a ship-wake program, of which the work reported here is a part. At ORI researchers had been working on elucidating the physical mechanisms for radar imagery of ship wakes (Hoglund, 1983), with particular emphasis on narrow-V wakes (Witting & Vaglio-Laurin, 1985). We were tasked to examine the photography from the Space Shuttle Earth Observations Project of NASA, to elucidate major wake morphologies in the imagery, to offer simple interpretations of the imagery where possible, and to relate the physical processes that influence the optical imagery to SAR imagery.

Under different sponsorship an independent study of Space-Shuttle photographs is in progress (JASON, 1986), and has produced a great deal of insight (Munk, et al., 1987). The JASON effort has concentrated on a detailed case study of three consecutive Shuttle photographs, each containing the same three ships as viewed under different sun-ship-observer geometries. For this case study Munk, et al. have developed a reservoir of useful theory that we draw from in this study. The work reported here differs from the JASON work in including a much larger sample of ship-wake observations, with a concomitant smaller detail given to each one. Our results support the conclusions reached by Munk, et al. It turns out that the (conceptually) simple optical model of specular reflection is sufficient to interpret all of the imagery, so long as plausible assumptions about the ship-induced hydrodynamic disturbances are made.

The major topic of this report is the display and interpretation of a rather large number of Shuttle photographs (Section 4). Preliminary sections give some details on their acquisition (Section 2), and outline some basic theory involving optical scattering and ship waves and wakes, to provide a theoretical framework for interpretation (Section 3). Section 5 summarizes the interpretations and relationships to radar imagery.

2. PHOTO ACQUISITION

The collection of photographs to be described here are a small portion of those taken on Space Shuttle missions, which started in 1981. From the start of the manned space program visual observations revealed interesting ocean (and land) structures. Photography of the earth became a prime experiment for astronauts in orbit, with extensive training given them on the underlying earth sciences so that they could capture scenes of scientific interest and importance (see Munk, et al., 1987 for a brief history). Hand-held cameras of two types have been used on Shuttle missions: 1) NASA-modified Hasselblad 500 EL/M 70 mm cameras equipped with interchangeable lenses of focal length 50 mm, 100 mm, and 250 mm, and 2) a Linhof Aero Technika 4" x 5" camera with interchangeable lenses of 90 mm and 250 mm focal length. On the one mission that produced most of the photographs shown here, STS 41-G (flown October 5-13, 1984), a nadir-looking large format camera (LFC) was deployed external to the command module of the spacecraft.

The selection of photographs for closer examination was made by surveying NASA's collection of film and choosing a sample that showed ship-wake features most clearly. As expected from earlier observations in manned space programs, in general, wakes showed up best in sun glitter (as did the other oceanographic features observed, such as internal waves, swell, and spiral structures). Note the bias here, however, in that most of the oceanographic scenes recorded by the hand-held cameras were in sun glitter because the astronauts pointed the camera that way. They favored looking at sun glitter from previous experience that it is in the glitter that you see oceanographic features. We examined the LFC photos from mission 41-G, which generally did not contain any (or, at least, much) glitter, and discovered only faint, short ship wakes. This supports the observation that ship-wake visibility is associated with the ship's being in or adjacent to the glitter pattern.

The photographs selected for analysis were all taken with one of the two hand-held cameras. In each case the particular lens used was recorded. To identify the location of the scene (geographical coordinates through the photograph), and the lighting conditions (particularly solar elevation), requires some discussion. All the Shuttle missions flew in moderately low, nearly circular orbits, ranging from about 120 nm to 180 nm nadir distance. For each a good ephemeris is available (satellite location as a function of time).

A scene can be identified well if one of two sets of information is available: 1) a sufficient number of land features throughout the scene, or 2) the combination of both a good time at which the photograph is taken (within one second or so, through which time the satellite travels about four nautical miles) plus the look direction and orientation of the camera. The later Hasselblad photographs (mid-1984 and after) have the time that a picture is taken inscribed on the frame (to the nearest second); the earlier Hasselblad photos and the Linhof photos do not. When the time is available, the solar inclination (complement of the optical angle of incidence) is known precisely, and so, because the solar point appears on the photo, we can decipher the geographic position of one point on the photo. To complete the description without a land feature one can assume that the astronaut attempted to align the "top" of the photo to be parallel to the horizon. There is some uncertainty in whether the astronaut always made such an attempt, however. In the best-analyzed set of photos, those treated by Munk et al., (1987), which took advantage of the numerous islands in the scene (but were without a clock, since the photos employed the Linhof camera), the horizon was approximately 10° out of parallel.

For analysis the location of the sun (on the image) and its approximate elevation are the most important features. In all but three of the photos to be discussed these are known from knowing the ephemeris and time, or deciphering the time using island or other land features. Except for one photograph the angle of incidence of the sun is within a few degrees of 50°. The reason for this relatively tight range of lighting conditions at the time the astronaut chose to take a picture of an ocean scene is not clear (for scenes of land the range of angles was much greater). Possibly 50° is best for highlighting oceanographically interesting features. More likely, however, it is related to the fact that the satellite assumed a canonical attitude, placing the window through which the astronaut took photographs at a particular orientation with respect to nadir. This is a matter that should be investigated further.

A typical photograph shows a sun-glitter pattern, and the angle of incidence of the sun's rays are approximately known. From the known camera focal length and aperture, as well as approximate camera orientation, one can estimate distance scales on the image, the estimate being best in the vicinity of the glitter pattern. In each photo we display approximate scales that apply near the center of the photo. Due to uncertainties in camera orientation, and, in some instances, an approximate time (needed to determine

solar angle), the scales are not precise to better than 20%. In the following analyses, however, no conclusion depends on higher accuracies than this.

Though all the available mission photographs were examined, the collection of photos in this report come from four missions: STS 41-B (February, 1984), 41-C (April, 1984), 41-G (October, 1984), and 61-A (October-November, 1985). For each Space Shuttle mission NASA produces a data report giving much of the basic information for each photograph. After our selection of ship-wake photographs, we consulted the published reports (Palmer, 1984; Nowakowski & Palmer, 1984; Hughes, et al., 1986), and were provided the data for Mission 61-A from CDR Donald Mautner, Navy liaison officer at the Johnson Space Center. High-quality prints from the original negatives were obtained through processing at the NASA/JSC photo lab, with special instructions to bring out the ship-wake features of interest. Typically, this overexposes the scene as a whole. From these prints we produced, and display in this report, a deliberately light xerox copy for annotation and discussion. Many of the underlying features are very faint or are not visible on the copy in this report. Full identification of each frame is given, however, and the interested reader can order slides or prints of each photograph from:

U. S. Geological Survey
EROS Data Center
Sioux Falls, SD 57198
Telephone Number: (605) 594-6151.

For a full appreciation of the information content in the photos one must consult high-quality prints or transparencies of the original photographs, and we have found it impossible to describe fully the richness and subtieties that appear. Nevertheless, we are able to describe the major features of each photograph and are able to interpret these features with geometrical optics, elementary theory of the wind-driven ocean surface, and plausible conditions for ship wavemaking.

3. THEORETICAL BASIS FOR INTERPRETATION

The Space-Shuttle photographs have been examined by several researchers, and some interpretations have been published (Munk, et al., 1987, Scully-Power, 1986, Hughes, et al., 1986). All of the interpretations, including our own, rely on geometrical (ray) optics as the sole imaging mechanism. Thus, all reflections from the surface are specular, in contrast to SAR imagery, where the wave properties of the electromagnetic signal, which are responsible for Bragg scattering, play an important and frequently dominant role. The simplification in the optical case occurs because the wavelength of light (the order of 1/2 micron) is small by comparison with all surface-wave scales.

The optical imagery, however, is intrinsically bistatic, in contrast to SAR imagery. In place of the backscatter radar's single angle of incidence, the bistatic geometry involves three angles: two angles of incidence, one of the source (usually the sun) and the other of the receiver (the camera), as well as an azimuthal angle that represents how out-of-normal are the ocean surface and the plane defined by the sun, reflecting point, and camera. To fully interpret a photograph requires the considerable effort expended by Munk, et al., who state: "It is a matter of a rather heroic application of elementary geometry [to make the coordinate mappings for quantitative analysis of wakes in the photographs] and we will not bore the reader with details; the relevant formulae and numbers are given in the appendix." In dealing with the larger sample we seek a simpler framework for qualitative interpretation and find this by considering more idealized geometries.

A. Basic Imaging of the Kelvin Waves

Figure 3 places 12 reproductions of the ship wake shown in Fig. 1, each oriented in the same direction, but arranged around a central point (the "sun"). For simplicity, imagine that a camera looks down on the scene from a finite height, with a faraway (infinitely far), point sun directly overhead, and no other lighting. Also imagine that the ocean surface is a perfectly flat reflecter. Then the center point in the scene would be bright, and all others would be dark. With one of the 12 ships present it may be possible that sunlight, still coming from directly overhead, reflects off of a section of a wave near the ship toward the camera, shows up as another point. From a wave train there can be many such specular points, and the collection of points can form a pattern on the image.

One can think of the ship waves as a collection of a large number of individual plane waves, and the pattern as the result of the destructive interference of most of these. Beyond a relatively small distance behind the ship each small region in x-y space is occupied only by wavenumbers near a single pair (or none). The mapping of one member of the pair is the transverse pattern, and the other is the divergent pattern. Frequently one of the patterns dominates, as the divergent one does in Fig. 3. Under these circumstances, there is a one-to-one mapping of location (x and y) and vector wavenumber (k_x, k_y). Therefore, in deciding whether a point in the Kelvin-wave pattern might be a specular point, we can think of a point in the pattern as being occupied by a plane wave of specific amplitude, wavelength, and direction.

A light ray coming straight down onto a level surface is deflected by a wavy surface, and if the wavy surface is a plane wave, each light ray has to be deflected in the plane that contains the incident ray and the surface wave-vector. The amount of angular deflection is twice the local water slope, and so the sum over a wavelength on the surface is a domain of outward-going radiation shaped like a hand-held fan, the fan half-angle being twice the maximum surface slope of the wave.

Referring to Fig. 3, note that reflected light can reach an observer located above O only if, from his viewing, the waves in the Kelvin wave pattern of the ship are pointed toward him, for otherwise the plane of the fan does not intercept him. In addition, the fan must be open enough to intercept the observer--this requires the combination of waves of large enough slope and an image (angular) location near enough to the center. When both conditions are met--the proper orientation of the Kelvin waves and sufficient amplitude, exactly one point per wavelength will be specular and will be imaged as a bright point. A localized wavetrain will be imaged as a succession of points along a straight line. With blurring over the scales of a wavelength, these specular points will merge to form a straight line, and with such blurring all information about the wavelength is lost. To say this another way, wavelengths in the Kelvin-wave pattern should not matter--only the wave orientation and slope matter.

It is clear that the directionality condition can be met only if the Kelvin wavevectors are pointing directly toward or away from the center point of Fig. 3, i.e., lines of crests are oriented tangentially. For clarity we have shown relatively large patterns in Fig. 3. Imagine that these patterns are shrunk, so that each pattern contains

many more waves than are shown, and that the pattern as a whole is smaller. Then a radial line from the sun to a particular ship would intercept all points in the wake at nearly the same angle with respect to the ship's direction. Now all the waves in a particular ship-wave pattern (transverse or divergent) have the same orientation with respect to the ship-direction *along radial lines drawn from the ship*, and the orientation is a single-valued function of ship-radial direction. We would expect that the condition that the ship wave be oriented correctly for specular reflection means that specular reflection points lie along a (single) radial line from the ship (or are absent). We would, in this idealization of a flat sea and a point sun expect that the image of the ship waves, if present, would be a straight, bright line, from the ship to a distance behind, stopping abruptly at the point the wave-slope is no longer enough to produce a specular point.

The optical situation is more complicated than described above in the following ways: 1) The sun is not a point source, but presents a disc of small (0.5 degrees) diameter to the earth. 2) The ocean surface is not flat in the absence of ships, but (usually) is filled with wind-waves. 3) The sky is also light. 4) The sunlight is not at zero incidence angle. The first two of these complications show up as an extended sun-glitter pattern on a photograph. In the limit of winds so light that waves have negligible slope, the sun would still occupy a 1/2 degree disc on the photo. For more realistic winds the glitter pattern would be much larger. Cox and Munk (1954a, 1954b) did the classic (and still unmatched) work on relating oceanic glitter patterns to wave slopes and winds. A theoretical shortcut that relates windspeed to wave-slope variances is given in Appendix B. In any event, the effect of an extended sun is to broaden the width of the image-line by superposing lines to all points where there is sunlight. Consequently, what would be imaged from a ship would be a radial fan.

Each ship in Fig. 3 is marked by solid or dashed lines. A solid line shows the positions where divergent Kelvin waves would be imaged, assuming, of course, that the ship generates them. The solid lines shown for the 60°, 120°, 240°, and 300° ship positions should be strong. Those for the 90° and 270° ship positions would probably be very faint or absent, because ships make tiny divergent waves on the center line. The dashed lines do not meet the criterion of imageability from zero-extent glitter patterns, but show the region(s) of the ship wake that would be most strongly imaged with appropriately broad sun glitter. For all angles except 0°, 90°, 180°, and 270° the triangular region where Kelvin waves can exist lies asymmetrically about a radial line

drawn from the solar point, and the preferred imaging region is on the side more perpendicular to this radial than the side more parallel.

Figure 4 shows one pair of divergent and the nearest transverse wave crest, taken from Fig. 2, placed in our nadir solar geometry. Locally, all waves in the vicinity of the line are directed normal to the line. The direction normals (facing both ways) cover the entire plane. Therefore, no matter how the ship is oriented with respect to the solar direction, there is one (and only one) radial line from the ship that could be imaged (if the waves are large enough) in the canonical geometry. In the vicinity of 0° and 180° in Figure 3 this is along the center line, but it is the weak transverse wave pattern that provides the correct geometry. If the crest line pattern of Fig. 4 is laid in each of the ship positions of Fig. 3, it is easy to see that, no matter whether it is the divergent or transverse wave pattern providing the required slopes, the conclusion of the last paragraph holds: the side of the wake that is more favorable for imaging is that more perpendicular to the sun-ship radial.

The fourth complication above, that the sun is not directly overhead, has been dealt with masterfully by Munk et al. (1987), who perform calculations with an arbitrary solar angle of inclination. Qualitative results from their work can be summarized as accounting for only a distortion of the picture shown in Figure 3. Let us imagine a photograph that contains a resolved glitter pattern and a (perfectly resolved) ship wake at some radius and azimuth from the glitter pattern. Place the solar point in the photograph at the center of a mimic chart and the ship at the corresponding point. A glitter pattern that would be circular when viewed from overhead (assuming that wave slopes are isotropic--not a bad assumption) becomes elongated when the sun is at non-normal incidence, becoming extremely elongated at grazing incidence. Similarly, the Kelvin wake becomes increasingly distorted with increasing solar angle of incidence. Nevertheless, (reasonably short) straight lines marking particular Kelvin wave angles still map to straight lines, though the angle between two lines is a function of solar elevation and an azimuthal angle. The entire view shown schematically in Fig. 3, while approximate as far as wake-angles and the precise location of wave directions relative to location in the wake are concerned, is qualitatively correct. Specifically, a "strong-imaging" line exists in asymmetrical geometries, and in a photograph taken with any solar inclination this line is more nearly perpendicular to a radial from the sun than that corresponding to the other side of the wake centerline.

The above discussion is relevant [illegible] pattern, where a wave aligned in favorable geometry adds [illegible] absent before. We also have a few examples where a [illegible] very close to the center of the glitter pattern appears dark [illegible] scattering out of specular points. These need not be tuned [illegible] direction. Rather, a dark line near the center of the glitter [illegible] manifestation of large-amplitude waves near the cusp draining the [illegible] scatterers. The same phenomenon occurs for the ship [illegible] important there.

B. Turbulent Wake

The manifestation of the turbulent wake of a ship is frequently the longest [illegible] feature imaged. Its basic appearance depends on its location in the glitter pattern, being darker than the immediate surroundings at the edge of the glitter, and brighter than the surroundings near the center of the glitter. When it is a dark feature, it may be accompanied by a brighter edge on one or both sides.

While the detailed physical interpretation of ship wakes and their effect on ambient waves is complicated and not known in perfect detail, it is observed that the surface waters of the ship wake are smoother than the adjacent waters. Evidently the turbulent motions in the wake, or the wake's mean currents, damp or reflect incoming water waves to produce the smoother water. It can sometimes occur that incoming waves are blocked near the edge of the wake. Thus, a turbulent wake is smoother water, sometimes with rougher edges.

The optical signature of a patch of relatively smooth water in glitter depends on location in the glitter. Figure 5 sketches the optical intensity of light coming from a line through the center of a glitter patterns produced by ocean surfaces of differing mean square slope. At the center of the pattern the brightness is greatest for small slopes, because all the reflected light is confined to a small angular region. At distances larger than that where the lines cross, the brightness is greatest for large slopes, because the reflected light spreads to the required distance only for larger slopes. Consequently, we would expect that smooth water would image bright near the center of the clutter, and dark at the clutter's edge. This is precisely what we shall observe in the photographs,

both as a general trend in the collection of imaged ship wakes, and for the occasional individual wake that spans both the center and the fringes of the glitter pattern.

C. Effects of Realistic Kelvin-Wave Patterns

Two important aspects of actual ship waves need some discussion. The foregoing discussion concentrated on directionality of Kelvin waves, but clearly their amplitudes are also important. When the sun-glitter pattern without ship is broad, the appropriate fan marking a ship signal acquires a (broad) finite thickness. Thus large-slope Kelvin waves can be imaged if even the edge of a thickened fan intercepts the camera. Because wave slopes just inside the cusp of the Kelvin-wave pattern are much higher than those further inside, they might be imaged more strongly. On average, we should expect preferential imaging of regions of the ship waves near the cusp.

Many of the Kelvin-wake images show several distinct bright lines fanning out from the ship. In keeping with our notion that there is a single preferred line for the imaging of asymmetrical Kelvin-wave patterns, we call this "line-splitting." This aspect of optical imagery was investigated in detail by Munk, et al. (1987). They explained the formation of multiple lines fanning out from the ship as being the result of the interference of Kelvin-wave patterns by multiple-sources associated with the ship motion. They showed that a double source was able to split an image line into three lines or so, and surmised that the complicated real flow around a ship could be responsible for the observed multiplet line splitting.

To sum up: we can think of the image of Kelvin waves as the radial line that would exist with a point sun and flat ocean, having a length proportional to the wave amplitude in the particular imaging direction, broadened by finite-sized sun glitter, and split into a multiplet radial line structure by complexities in the ship's wavemaking.

4. SHUTTLE PHOTOGRAPHS

Table 1 summarizes the more relevant parameters of the photographic collection shown as Figures 6-34 of this report. The 29 photographs were taken from four missions, and most of the information in Table 1 is found in Palmer (1984), Nowakowski & Palmer (1984), Hughes, et al. (1986), Munk, et al. (1987), and private communications with Ken Hancock, NASA, and CDR Donald Mautner, USN. We offer here a commentary for each photograph or set of photographs, based on examination of high-quality prints with the interpretive framework provided in Section 3. On each figure are drawn line patterns to identify each ship observed. The solid lines, which are bright except where noted, represent our identification of a Kelvin-wave feature. The dashed lines, which are darker than the surroundings except when near the center of the glitter pattern, represent our identification of a turbulent-wake feature. For clarity, we shall use the word "Figure #" to refer to a particular figure in this report, and "Photo #" to refer to the corresponding high-quality print that we examined.

Figures 6-8 show the same ship under three lighting conditions. The ship and Kelvin-wave feature are extremely faint in Photo 6. The (dark) turbulent wake in Photo 6 has a light (near) edge. The Kelvin-wave feature in Photo 7 is in the same relative location to the wake as it is in (6), but is now a dark feature in the bright glitter. This feature shows clearly and bright in Photo 8. In Fig. 8 note that the Kelvin-wave arm shown is the one more perpendicular to the radial from the center of the glitter. In this photograph we have a clear manifestation of the conclusion of Section 3 that it is this side of the Kelvin wave pattern that should be imaged preferentially. As we go through all the figures, we shall find that this is true for all the Kelvin-wave features shown as a solid line. The noteworthy feature of these images is the length of the turbulent wake. Not only is it longer than the Kelvin-wave feature, but it is long absolutely--approximately 50 n.mi. in Figs. 6-7. Except for rather obvious cases where the ship has been discharging oil or some other slick-making substance, this is as long a turbulent wake as we have observed.

Figure 9, which shows two ship images, has a rather large and complex glitter pattern. Ship B has a more complex multiplet structure than is indicated, expecially in the vicinity of arm BY, a dark line appearing that may be part of the multiplet structure but might be the turbulent wake. In any event, ship A images well in the broad glitter

pattern. Munk, et al. (1987) have suggested that optical imaging of ship wakes is favored by low wind conditions. If we interpret the broad glitter pattern of Fig. 9 as indicating wind speeds of 10 m/s or more (see Appendix B), then we have an example of good imaging in strong winds.

Figs. 10-11 show the same ship, A, under different lighting conditions. Photo 10 shows a multiplet structure, more pronounced near arm AZ, which is considerably brighter than arm AY. Adjacent to ship A are a pair of bright features that might be ships, but look like no others seen in the collection. These have not been annotated. The noteworthy feature of this pair is the presence of a cluster of about four ships, marked by B in Fig. 10, that do not appear in Photo 11. The reason is clear--the location of these ships in Photo 11 is in a patch of blackness. Even though the sun-glitter is not far away, no image appears. In Photo 10 the imaged features are rather short, even though the lighting is very favorable. Evidently, the ships are small or are traveling slowly, so that their Kelvin waves are relatively low-amplitude. Thus, in Photo 11 their slopes are insufficient to reflect light even through the small angles necessary to reach the camera.

Figure 12 shows two ships with Kelvin wave features against a very dark background. The longer arm of each is also the brighter by far. In contrast to the absence of an image of the cluster of ships in the darkness in Photo 11, these presumably larger or faster ships image well.

Figure 13 shows a complex scene with six ships identified. In Photo 13 the Kelvin-wave imagery is rather diffuse. The region between the bright arms is also brighter than normal, and the bright arms themselves are not much brigher than this wedge-shaped region. The identification of AY as a turbulent wake would be marginal if it were not for its probable extension through YY'. The identification of BY as a turbulent wake is less uncertain on its own, and is confirmed by its probable extension YY". That DY is a turbulent wake is not certain. The morphology of the Kelvin-wake features from ship F is rather distinctive. A multiplet structure clearly shows up, with a definite discontinuity in the orientation of the lines on the side FZ. This is similar to the famous SEASAT Rev. 407 image.

Figure 14 contains two interesting ship images. Ship B is somewhat mysterious. The bright line BY is a canonical-looking Kelvin-wave feature. Yet the feature Y'Z in

Photo 14 is a pair of thin dark lines that look like a turbulent wake. Two possibilities present themselves: 1) Line BY is actually a (bright) turbulent wake that continues to Y'Z, or 2) line Y'Z is some feature not related to ship B. We favor the latter possibility. The ship at A, which is distinctly dark in the photo, makes a turbulent wake that goes straight through the discontinuity in both brightness and color that runs diagonally from lower left to upper right in Photo 14 and is clear at the lower left of Fig. 14. It is difficult to imagine an oceanic front or other feature that would not shear a "stripe" painted along the ocean surface. We believe that the discontinity in background brightness and color marks an abrupt atmospheric, not oceanic, discontinuity.

Figures 15 and 16 show ships against an unusually orderly glitter pattern (almost circular and with brighness distribution less patchy than normally seen), but with an unusually intense imagery of spiral structures. The two photos were taken only 5 seconds apart, and, if the camera were oriented the same (with respect to the space craft), there should be considerable overlap in the photos. Indeed, the relative locations and appearances of two of the ships in each image is similar (15-A and 15-B compare to 16-C and 16-D). If we assume that the these pairs of ship-images are of the same pair of ships, however, too much would need to be explained away, notably the absence of similarity in the corresponding eddy patterns and the absence of any hint of ships E and F in Photo 15. We tentatively regard the scenes as separated, therefore.

Our identification of Kelvin-wave features with solid lines and turbulent wakes with dotted ones is rather tenuous in both Figs. 15-16. It is true that some features resemble those seen elsewhere, e.g. the multiplet structure of 15A toward the direction AZ, dark spots in bright glitter marking the ship locations 15B, 16C, 16D, 16F, and others. Even so, due to subtleties that we find it difficult to describe, we regard the appearance of the ship features in these two photographs as exceptional, and worth examining further.

Figure 17 shows a V-wake with uneven arms. Because Photo 17 was taken 31 seconds after Photo 16, we do not think that the ship of (17) is any of those in (16) or (15). The longer, brighter arm of the V may be split. This ship image possesses higher contrast than any we have encountered. From the discussions in Section 3 we do not find this surprising, in view of the extreme closeness of the ship to very bright glitter, itself

being in a dark patch of water. It would not take much Kelvin wave slope to produce facets aimed at the camera where none were aimed without the ship.

Figures 18-20 show long features of good contrast. The single oceanic feature in Photo 18 is probably a slick, perhaps laid down by oil discharge from a ship. The abrupt beginning of the feature is broad and we see no ship associated with it. It does not look like any of the turbulent wakes of the ships displayed thus far. We shall discuss this photo in connection with a later sequence, (Figs. 25-27). Photos 19-20, which were taken 11 seconds apart, show the same ocean region in somewhat different lighting. Photo 19 clearly shows a dark ship at A. No ship is seen connected with B or C on either photo. For this reason the associated ships (if, indeed, these are ship wakes) are denoted as being off the photos. The three features associated with A, B, and C are indicated as being ship wakes. If one looks at either Photo 19 or Photo 20, but not both, he would say "clearly ship wakes," based on their appearances. The A-ship feature is bright in Photo 19 and dark in Photo 20, while the features associated with B and C are dark in Photo 19 and bright in Photo 20. This sense entends throughout their entire lengths. Now these lengths span a greater lighting contrast than is evident between corresponding lines in the separate photos. In addition, the strong eddy structures that show up ahead of A (in both photos--here best seen in Fig. 20) have the same sense of brightness, i.e. the thin filaments are dark in both. Yet the eddies that show up along the tracks of A, B, and C have opposite senses of brightness, i.e. the thin filaments are light in Photo 19 (see Fig. 19) and dark in Photo 20, the same sense as the feature behind ship A.

Figures 21 and 22 show the same scene from photographs taken 4 seconds apart. Unfortunately, the prints were made at different times, and one is reversed relative to the other. These show a great deal of richness and variety. The common feature in the photos are the three lines trailing behind A, J, and K. In Photo 22 the ships associated with the A and K lines are observed as dark spots, as is the ship at L. The ship at J has very faint Kelvin wave features that enable us to identify its presence in the wake of L. In (22) there is a short, bright Kelvin-wave feature with A and a dark one associated with K. The track A is more intense than are the others. While tracks J, K, and L are dark on both photos, that of A is bright when the background lighting is strong, and this occurs more for Photo 21 than Photo 22. Photo 21 also contains many other ship wakes, including multiplet structure (ship D), and rather wide arms in the flotilla marked by "I".

Figures 23 and 24 show relatively weak Kelvin wakes of a single ship. The novelty in these photographs is that they also show a part of the United States (Long Island).

Figures 25-27 show a wide-angle view (50 mm lens) of an oil slick off the coast of Libya. After review, we discovered that Fig. 18 is a closeup view (250 mm lens) of the same slick) taken slightly before the Figs. 25-27 sequence. The timing is as follows: Photo 25 was taken two seconds after Photo 18; Photo 26 six seconds after Photo 25; Photo 27 ten seconds after Photo 26. The imaging is canonical: it appears light in strong glitter and dark in moderate to weak glitter. Somewhat more than 50 nautical miles of track are imaged by these photographs. The appearance of the oil slick differs from that of a ship in that the slick, though basically a linear feature, is considerably broader than the ship wake.

Figure 28 views the English channel between Dover and Calais. Unlike all other photographs in this collection, the view is not in or near sun glitter. Nevertheless, numerous surface ships are imaged, showing up as white specks. Although the images are small, they give a strong impression of ship bearing, being elongated and having a bright forward side. The imaging is probably due to both solar and sky reflections from the ship and the white-water near it and in its wake. Figure 29 also shows features against a relatively uniform lighting. One gets the impression that the ship at A (itself discernable as a dark speck in Photo 29, but very faintly) was discharging something between B and C. Many other features show up in the photo, probable ships at D and E, as well as wispy, faint, light features scattered about that have no obvious interpretation. These latter features remind us of the unmarked prominant features in Photos 10 and 11.

Figures 30-34 show a sequence that includes, importantly, the three ships marked as A, B, and C. These are imaged most clearly in Photo 32, and offer the clearest example of multiplet line structure. Munk, et al. (1987) selected Figs. 30-32 for their thorough analysis. Without making the simplifying assumptions we made in Section 3, they interpret the imagery of ships A, B, and C solely in terms of geometrical optics, with the proviso that the ship needs to make a Kelvin-wave pattern sufficiently complex that interference leads to extensive line-splitting. Ship A continues to be imaged in Photos 33-34, though weakly. In addition, Figs. 32-34 show a probable fourth ship, D, that is imaged a little further away from the strong glitter to the North.

5. SUMMARY AND CONCLUSIONS

This is the final report of a project to 1) examine Space Shuttle photographs and select those most suitable for studying ship wakes, 2) interpret the observed imagery of the ship wakes, and 3) relate our insights to Synthetic Aperture Radar imagery of ship wakes. We selected 29 hand-held photographs, which were taken during four Shuttle flights, as our study-set. Although some observed features are still unexplained, the vast majority of clear ship-wake images are explained by simple (in principle) geometrical optics. Both the astronauts' experience and our theoretical interpretation conclude that ship wakes are best seen in sun glitter, though ships are sometimes imaged well away from glitter.

Three features from ships are seen optically. The most persistent results from the turbulent wake of the ship. Its image shows up because of a smoothing of the ocean surface, appearing brighter in strong glitter and darker in weak glitter. Lengths can range to 50 nautical miles. Without another ship-related feature in the scene, such as the ship itself, or a Kelvin-wave line or fan, one cannot be sure that an observed ribbon is indeed associated with a ship. Second, various image morphologies result from the Kelvin-wave pattern of the moving ship. The variety results from the dual requirements of the ship-sun-spacecraft geometry and details of ship-wave amplitudes in all possible directions. The notion that the geometry establishes a particular viewing line on a photograph, which is spread into an angular region by surface roughness (and solar size), and is line-split into multiplets by detailed ship-wave interferences, appears to be sufficient to explain the basic Kelvin-wave features observed throughout our data set. Finally, when a ship is in especially bright glitter, it can show up as a dark spot, and when the ship is in skylight, it (and nearby breaking waves and foam) can show up as a compact light region. This "point" imaging is not as prominent in our collection as are the features due to turbulent wakes or Kelvin waves, but may be relatively more prominent under more uniform (and more typical) lighting conditions.

A. Relationships between Optical and Radar Imagery

After examining the photographs taken with both the hand held camera and the large format camera, we offer the following comparisons and contrasts with Synthetic Aperture Radar imagery.

1. Only geometrical optics needs to be invoked in constructing a satisfactory imaging model, and so surface reflections are specular. This contrasts with SAR theory, where imaging models usually need to account for Bragg scattering, i.e. one must account for the wave nature of the electromagnetic radiation. Indeed, through a range of incidence angles greater than about 20° Bragg scattering is more important than specular scattering. Furthermore, the specular scattering of radar waves by a rough surface should exclude those at the scales of the radar wavelength and smaller, and these small scales can account for a large fraction of the surface slope variance. The radar scene should become more similar to the optical scene as both the radar angle of incidence and radar wavelength decrease.

2. The optical observations are taken in a bistatic geometry. This contrasts with the backscatter radar observations, which are monostatic. While the bistatic geometry can be dealt with *a la* Munk, et al., the monostatic geometry is much simpler to deal with. The optical geometry tends to monostatic, however, in the limit that the sun is at nadir.

3. The most striking and unusual manifestations of ship waves for both optical and radar observations occur in light winds. The particular manifestations are different, however. In optical imagery both the striking multiplet structure and intense wake-arms of high contrast are seen best against a dark background just outside the brightest part of a small glitter pattern, the latter a manifestation of low local winds. In SAR imagery it is the narrow-V wakes that are the striking and unusual features, and these are definitely low-wind occurrences.

4. Manifestations of turbulent wakes are the lengthiest feature associated with both optical and radar imagery. In the photographs these appear best in a broad, but still definite, glitter pattern, suggestive of moderate winds. Long turbulent wakes in radar imagery are also seen preferentially in moderate winds, particularly in Shemdin's Gulf of Alaska experiments. The single most important factor responsible for optical wake imaging is the local smoothing of the surface. Before constructing elaborate theories involving radar-particular imaging mechanisms to explain turbulent-wake observations, one should see how far simple local smoothing will explain the imagery.

5. The multiplet structure of optical imageries is largely absent from radar imagery. This may be due, in part, to the lower spatial resolution of the radars. Nevertheless,

multiplet structure has been seen in radar imagery, e.g. SEASAT Rev 407, leading to much speculation about the cause. This similarity between optical and radar imagery suggests a possible common cause. We favor the Munk et al. theoretical framework, which involves interference sub-patterns in the pattern of surface waves from the ship.

B. Recommendations for Future Field Experiments

Enough information has arisen out of this modest effort to warrant two specific recommendations regarding future observational programs, one optical, the other radar. These are discussed in turn.

Our experience in viewing the Space Shuttle Photographs is that there is an enormous wealth of information in sun-glitter scenes that, however, is very hard to extract because of difficult (and uncertain) geometries. These scenes involved a hand-held camera. In later missions the time to the nearest second was noted, but not the camera orientation. Thus, unless several land features appeared in the image, it was impossible to decipher the scene's geometry precisely. But all scenes involving several land features also involved complex sun-glitter patterns, presumably because of gusty and nonuniform winds, and, possibly, patchy surfactants. We found the scenes in the large format camera far easier to interpret, because the camera pointed almost straight down and clicked at precise times. Unfortunately, the sun was never within 25° of normal incidence, and so ship wakes were very rare and were not seen in the best light.

We recommend an optical mission that 1) has the sun directly overhead, 2) looks straight down with a camera fixed to the platform, and 3) takes enough pictures to view the same part of the ocean surface in two or more successive frames. A sun-following aircraft mission should be ideal. The airplane would fly at local noon a course along the latitude of the sun. This would involve flights at Mach 1.5 or so, the exact Mach number depending on time of year (determined by the latitude) and altitude (to some extent dependent on the particular aircraft employed). Plenty of interesting ocean can be viewed, e.g. the trade wind stretch of the Pacific Ocean between Mexico and Hawaii.

The richness of the optical imagery in sun glitter suggests that the analogous radar imagery should also be rich. The analogy would be best if the radar scattering were purely specular and encompassed all scales of ocean surface variations. The radar

best suited would be nadir-looking and high-frequency. We recommend, therefore, that during upcoming aircraft SAR flights, some X-band imagery of surface ships be taken with the smallest incidence angles possible. We see no reason why Bragg scattering is necessary (or even the most easily interpretable) for viewing hydrodynamic features. It may turn out that near-nadir is not the best angle for viewing ship wakes with radars, but one can look near-nadir with some confidence that ship-wakes will be imaged.

C. Acknowledgements

We acknowledge the gratious assistance provided by the staff of NASA's Johnson Space Center in this study. Special thanks are offered to CDR Donald Mautner, USN, for his assistance in screening and securing the images, and to Professor Walter Munk for providing us with an early copy of his Bakarian Lecture, as well as for several enlightening discussions.

APPENDIX A--A NEW VERSION OF LINEAR SHIP-WAVE THEORY

In this appendix we sketch the development of a version of linear water wave theory as applied to a simple source (ship) moving at constant speed through the ocean. The problem addressed is not new; Kelvin (1887) gave a solution. What is new is the method of solution, which exploits modern high-speed computers and an efficient algorithm (Fast Fourier Transform). Originally developed by Witting & Vaglio-Laurin as a rapid and convenient tool use in analyzing SAR images of narrow-V wakes, we now find that it has more to offer than convenience, namely, better accuracy in the regions closer in to the ship than can be reliably described by the usual asymptotic theories.

The equations of continuity and of motion for flows in an incompressible inviscid fluid with a free surface are:

$$\partial\eta/\partial t + \mathbf{div}\ \mathbf{M} = Q \tag{A.1}$$

$$\partial\mathbf{u}/\partial t + (\mathbf{u}\cdot\mathbf{div})\ \mathbf{u} + \mathbf{g} + (1/\rho)\ \mathbf{grad}\ p = \mathbf{grad}\ R \tag{A.2}$$

where the following notation is used:

- η elevation above a horizontal reference plane, e.g., still water
- $\mathbf{M}$ volume transport
- Q source of volume
- $\mathbf{u}$ fluid velocity at a point
- $\mathbf{g}$ acceleration of gravity
- ρ fluid density
- p fluid pressure
- R source of momentum.

Two major simplifications are made at this point: (1) The above equations are linearized, and (2) the zeroth order velocity field is no more complicated than a uniform flow, which is taken to be in the x-direction. Then (A.1) and (A.2) become:

$$\partial\eta/\partial t + U\ \partial\eta/\partial x + \mathbf{div}\ \psi_S = Q(x,y,t) \tag{A.3}$$

$$\partial\phi_S/\partial t + U\ \partial\phi_S/\partial x + g\eta = R(x,y,t) \tag{A.4}$$

where ϕ is a velocity potential for the perturbation, ϕ_S being its surface value, ψ_S is the perturbed mass transport (a vector), and U is the unperturbed fluid speed. Eq. (A.4) is a Bernoulli law, and is valid for an irrotational flow.

Equations (A.3-A.4) contain three field variables, and a third equation is required to close the system. This is Laplace's equation for the velocity potential $\phi(x,y,z)$, with the boundary condition that it vanishes at great depth ($z \to -\infty$). In Fourier space (with a "hat" over a variable denoting its Fourier transform) one can derive the desired relation

$$\mathbf{k} \cdot \hat{\psi}_S = -i \, |\mathbf{k}| \, \hat{\phi}_S \tag{A.5}$$

where the sign convention in defining a direct Fourier transform is $\exp(+i\mathbf{k}.\mathbf{x})$, as in Morse & Feshbach (1953).

Ordinary ship waves result from the forces imposed by the ship on the ocean that are steady in the coordinate system moving with the ship. All waves generated by the ship are steady in these ship coordinates. Thus, we may set all time derivatives to zero and represent the sources as functions of x and y only. For simplicity, assume that Q vanishes, so that the only source is $R(x,y)$. The Fourier transforms of (A.3-A.4) with (A.5) lead to:

$$\hat{\eta} = k\hat{R}/[gk - (k_x U)^2] \tag{A.6}$$

where k is the magnitude of wave number $\mathbf{k}$, with similar expressions for the velocity potential, vertical and horizontal components of velocity, etc.

Equation (A.6) is appropriate for ship-imposed forces at the ocean surface. If the source lies at depth z_o beneath the surface, a reasonable model would include the factor $\exp(-kz_o)$ in the numerator of (A.6), as Lamb (1932) shows (but strictly only for large kz_o).

The elevation that results from a point force [$R(x,y)$ being a Dirac δ-function, giving $\hat{R}(k_x,k_y)$ a constant] is the fundamental (Green's function) solution. It is simply the inverse Fourier transform of (A.6), with a causality condition that the waves made by the ship lie behind the ship. The inverse transform involves a contour integral, with

causality determining the half-plane into which the singularities of (A.6), i.e. the 0's of its denominator, should be displaced by an infinitesimal amount. Analytic theories are faced with evaluating the integrals that result from taking the inverse Fourier transform of (A.6), or an equivalent integral. Because the last integral remaining has no known analytic evaluation, one resorts to approximation. All the approximations are asymptotic and drop terms of higher order in the parameter (1/N), where N is the number of waves between the observation point and the source. In ascending order of sophistication we have elementary methods of stationary phase as found in Lamb (1932) and, with more careful treatments of phase differences between divergent and transverse waves, in Stoker (1955) and Wehausen & Laitone (1960). These predict that wave amplitudes fall off as distance from the ship like distance to the -(1/2) power. The latter treatments account for the 90 degree phase difference between the two branches at the cusps, where they meet. These elementary methods fail at and near the cusps of the wave pattern, giving an (unwarranted) infinite amplitude there. Peters (1949) gives an asymptotic solution that predicts an $r^{-(1/3)}$ amplitude along the cusps, and Ursell (1960) constructs a more complete asymptotic theory, involving Airy functions, that goes from the cusps, where we have the (-1/3) power law, to a sufficient distance inside, where the power is (-1/2).

We adopt the alternative of inverting (A.6) directly, using two-dimensional Fast Fourier Transform (FFT) algorithms. For causality, we need to include a small imaginary part to the denominator of (A.6), and enough imaginary part needs to be included to prevent waves that leave the downstream side of the source to enter the box from its upstream side (periodic boundary conditions are employed). We put the particular wave-number-dependent imaginary term into the denominator of (A.6) that results in a particular damping of waves downstream, one for which *the decay rates of all linear waves, no matter what their two-dimensional wavenumbers, is the same.* This enables us to undamp the solutions in x-y space upon multiplication by a known exponential factor. To our knowledge, the only source of imprecision in these direct calculations is the finite resolution set by our having the equivalent of a mesh with finite spacing between mesh-points.

Sample calculations have been run at various resolutions, source-directions (relative to the axes defining the computational domain), and numbers of waves in the computational region. Figures 35-37 show sample results for a smooth source of dimension one grid interval (nonzero source strengths are located at a central point, its four nearest

neighbors, and the next tier of four points). The depth of the source varies from (35) to (37), with the divergent wave pattern dominating at zero depth and the transverse pattern at the larger nonzero depth. For surface ships the divergent waves dominate for fast-traveling (high Froude number) ships, and the transverse waves for slow-traveling (low Froude number) ships. Figure 38 is an illustration of how various mechanisms that occur for synthetic aperture radars would affect the imagery.

Some of the computer runs have been carefully examined. We find that at large distances from the source we are approaching the asymptotic results, e.g. $r^{-1/3}$ dependence along the cusps, and $r^{-1/2}$ dependence well away from the cusps. At smaller distances (a few tens of grid points) we see effects of finite resolution, but beyond this the results appear to be insensitive to resolution. From several tens of grid points from the source to the limit of the numerical calculations (256 x 256 grid points to date) differences between the numerical and the asymptotic results point to limitations in the asymptotic theories for sources located at finite distances away from the observation points.

We summarize the relationship of the new approach with the older asymptotic theories as follows: Very far from the source (hundreds to thousands of wavelengths) one can apply the asymptotic results with confidence, but Ursell's sophisticated theory is necessary near the cusps. Our direct methodology would require too much computer time to be competitive. At an intermediate distance from the source (tens to hundreds of wavelengths) one can obtain accurate results from either approach, and neither is particularly expensive. Nearer the source (a few tens of wavelengths away) the direct approach is the more accurate. Very near the source (one or two to a few tens of wavelengths) the asymptotic methods break down, but our direct method should be accurate to the extent that the calculations retain the necessary resolution. For source-strengths appropriate to actual surface ships, however, the accuracy of linear wave theory becomes suspect.

APPENDIX B--A SIMPLE MODEL OF WIND-DRIVEN SURFACE SLOPES

The optical imaging of surface-ship wakes is sensitive to the ship's being in or near a sun glitter pattern. The pattern is made by the reflection from the sun, whose rays are nearly parallel (within 1/2 degree). Specular reflection from a point on the ocean surface occurs if a ray's angle of reflection equals the angle of incidence and is in the plane defined by the local surface-normal and incident ray. To the first approximation, the angular distribution of the reflected radiation is a simple mapping of the directional slope distribution. For normal solar incidence the probability density function for radiation into a solid angle is just the probability density function for surface slope at half the corresponding polar angle. Thus, the properties of the sun glitter are, to the first approximation, a simple mapping of the probability density of surface slopes.

We assume that the surface slopes are due to a large number of waves, a sufficient number of which are uncorrelated so that the slope-distribution is Gaussian (in two angular dimensions). As we shall see, the higher frequency waves contribute the bulk of the variance in sea-surface slope, and these are thought to be nearly isotropic, i.e. do not depend on directions relative to the wind. Under the assumption of a Gaussian distribution and isotropy, the statistical properties of the surface slope depend on a single parameter, which we take to be the mean square surface slope. The task at hand is to develop a simple model relating this mean square slope to the wind.

The classic models that relate surface waves to wind speed and direction also need to take into account wind duration and fetch, but are rarely concerned with atmospheric stability. These models, however, are concerned principally with the longer waves in the spectrum. For the short waves the sea is "fully developed" at short wind durations and fetches. In constructing our simple slope model we do not consider any but fully developed seas (note, however, that recent independent laboratory experiments by Mark Donelan and by Norden Huang show that the high-frequency wind-generated elevation spectra are profoundly modified by paddle-generated long waves, and a more sophisticated slope model would need to take this into account). In addition, the atmospheric stability would need to be included. In the spirit of keeping our model simple, however, we shall derive a mean square slope that is related only to the wind speed.

In a fully developed sea the notion of a "saturated" or "equilibrium" part of the spectrum is useful, with spectral densities independent of wind speed. Considering the frequency spectrum of surface elevation one can write the Phillips spectral density in the form:

(B.1) $$\Phi(\omega) = \beta\, g^2/\omega^5$$

where β is a dimensionless constant, g is the acceleration of gravity, and ω is the (radian) frequency. Numerous laboratory and at-sea experiments are consistent with the form of (B.1) and give values of ω near 0.012 (Phillips, 1969). Recent research has pointed to deficiencies in (B.1), but we shall adopt it here.

Over the same range of frequencies that (B.1) is an adequate representation of elevation we take the slope spectrum to the that corresponding to (B.1) in the absence of (rather pathological) directional characteristics, i.e.

(B.2) $$\Psi(\omega) = \alpha k^2 g^2/\omega^5$$

where the constant α is the order of β, and k^2 here is meant only to be an indicator of the process of taking the magnitude of the spatial derivative of elevation. In the equilibrium range of the spectrum where short gravity waves dominate, frequencies and wavenumbers are connected by the dipersion relation:

(B.3) $$k^2 = \omega^4/g^2$$

One would expect that the form of the wave slope spectrum would be:

(B.4) $$\Psi(\omega) = \gamma/\omega$$

with γ being the order of 0.01. One can derive (B.4) directly by using the same dimensional arguments that lead to (B.1).

The spectra cannot be equilibrium at low frequencies, because the mean square elevation, which is the integral of the elevation spectrum between zero and infinite frequencies, would blow up. At frequencies near those at which the wind speed U and

wave speed g/ω are the same, the spectrum must start to depart from (B.1). The models that have been suggested (Pierson & Moskowitz, JONSWAP, and others) give a rapid falloff of the spectrum below this frequency. For our optical model we simply cut off (B.4) below this critical frequency, i.e. below:

(B.5) $$\omega_{min} = g/U$$

The spectrum (B.1) is integrable at the high-frequency end, but (B.4) is not, blowing up logarithmically. Consequently, we need to add some sort of high-frequency cutoff. Our choice is the frequency at which the growth rate of waves by the wind is balanced by the decay rate due to viscosity. The decay rate has long been known (see Lamb, 1932):

(B.6) $$\text{energy decay rate} = 4\nu k^2$$

where ν is the kinematic viscosity.

Knowledge of the growth rate has been accumulating in recent years; Plant (1982) has summarized his own and other data with:

(B.7) $$\text{energy growth rate} = 0.04\, u^{*2}\omega \cos\theta/c^2$$

where u^* is the friction velocity of the wind, c is the wave speed, and θ is the angle between the wind and wave directions. The data used to construct (B.7) are in the frequency domain of short gravity waves and extend into the capillary-wave domain, but do not go far into the capillary-wave region. For lack of anything better we postulate that (B.7) applies also to high capillary-wave frequencies.

Let us take the wave speed c that appears in (B.7) to be that appropriate for unadvected free waves, ω/k, and suppress the angular dependence by setting $\cos\theta$ to unity. Then equating (B.6) to (B.7) gives:

(B.8) $$\omega_{max} = 0.01\, u^{*2}/\nu$$

The mean square slope is the integral of its spectral density over all (positive by convention here) frequencies. From (B.4) with (B.5) and (B.8) we obtain:

$$\text{(B.9)} \qquad \langle \eta'^2 \rangle = \gamma \ln(\omega_{max}/\omega_{min}) = \gamma \ln(0.01\, u^{*2} U/g\nu)$$

To express uncertainties in our approximate treatment it would be best to replace the 0.01 in (B.9) with a constant. Moreover, for definiteness let us take u^* to be a fixed fraction of U, about 0.03 but dependent on atmospheric stability and, perhaps, wave duration and fetch. In addition, our postulate of an equilibrium region in the wave spectrum applies only when ω_{min} and ω_{max} are widely seperated. They are not well seperated at small windspeed, and (B.9) needs amending there. Taking these into account, we suggest the following form as a simple model to relate mean square surface slope to wind speed:

$$\text{(B.10)} \qquad \begin{aligned} \langle \eta'^2 \rangle &= \gamma \ln(CU^3/g\nu)\,; & CU^3/g\nu \geq 1 \\ &= 0 & CU^3/g\nu \leq 1 \end{aligned}$$

where C is a constant the order of 10^{-5} that is a function of atmospheric stability and the height above the surface at which U is defined. The table below shows some numerical values with $\gamma = 0.01$ and $g\nu = 10$ cm^3/sec^3) for widely seperated choices of C.

U (m/s)	$\langle \eta'^2 \rangle$		
	$C = 10^{-4}$	10^{-5}	10^{-6}
1	0.0230	0.0000	0.0000
2	0.0438	0.0208	0.0000
4	0.0646	0.0416	0.0186
8	0.0854	0.0624	0.0396
16	0.1062	0.0818	0.0615
32	0.1270	0.1040	0.0809

By comparison with the data of Cox and Munk (1954b), and with the photograph displayed as Fig. 9 of Munk, et al. (a 1951 photograph taken north of Hawaii with a wind speed of 4 m/s), it appears that a choice of C in the vicinity of 10^{-5} to 10^{-6} is reasonable. It should be noted, however, that the model of (B.10) is simplistic to an extreme, and that the properties of the sun glitter depend on more than the wind speed

alone, perhaps much more. Even so, this simple model has value in giving a rough estimate of wind speed from a photograph of sun glitter in situations were no other information on wind is available.

REFERENCES

Cox, C. S. & Munk, W. H. (1954a) "Measurements of the roughness of the sea surface from photographs of the sun's glitter," *J. Optical Soc. Amer.* 44, 838-850.

Cox, C. S. & Munk, W. H. (1954b) "Statistics of the sea surface derived from sun glitter," *J. Marine Res.* 13, 199-225.

Hoglund, R. F. (1983) "Selected SEASAT synthetic aperture radar images," ORI Report of 7 October.

Hughes, J., Gallagher, J. J., and Scully-Power, P. (1986) "Navy oceanographer Shuttle observations STS 41-G data catalog," NUSC Technical Document 7609 of 26 March.

JASON (1986), MITRE Corporation Report JSR-86-203 of August.

Kelvin (1887); see Thomson.

Lamb, H. (1932) *Hydrodynamics*, 6th Ed., Cambridge, Cambridge University Press; reprinted 1945, New York, Dover Publications.

Lighthill, J. (1978) *Waves in fluids*, Cambridge, Cambridge University Press.

Morse, P. M. & Feshbach, H. (1953) *Methods of Theoretical Physics*, New York, McGraw-Hill Book Co.

Munk, W., Scully-Power, P., and Zachariasen, F. (1987) "Ships from Space," The Bakerian Lecture of 1986, in press *Proc. Royal Soc. London A.*

Nowakowski, B. S. & Palmer, W. F. (1984) "Catalog of Space Shuttle earth observations hand-held photography: Space Transportation System (STS 41-C) Mission," Johnson Space Center Report JSC-20056 of September.

Palmer, W. F. (1984) "Catalog of Space Shuttle earth observations hand-held photography: Space Transportation System (STS 41-B) Mission," Johnson Space Center Report JSC-20038 of September.

Peters, A. S. (1949) "A new treatment of the ship wave problem," *Commun. Pure Appl. Math.* **2**, 123-148.

Phillips, O. M. (1966) *The dynamics of the upper ocean*, Cambridge, Cambridge University Press.

Plant, W. J. (1982) "A relationship between wind stress and wave slope," *J. Geophys. Res.* **87**, 1961-1967.

Scully-Power, P. (1986) "Navy oceanographer Shuttle observations, STS 41-G, Mission report," NUSC Technical Document 7611 of 26 March.

Stoker, J. J. (1957) *Water waves*, New York, Interscience Publishers, Inc.

Thomson, W. (1887) "On ship waves," *Proc. Inst. Mech. Eng., Popular Lectures*, p.482; also see "On the waves produced by a single impulse in water of any depth, or in a dispersive medium," *Phil. Mag. (5)* **23**, 252-255.

Ursell, F. (1960) "On Kelvin's ship-wake pattern," *J. Fluid Mech.* **8**, 418-431.

Wehausen, J. *V.* & Laitone, E. V. (1960) "Surface waves," in *Handbuch der Physik*, Berlin, Springer-Verlag, **9**, *Fluid Mechanics III*, pp. 446-778.

Witting, J. M. & Vaglio-Laurin, R. (1985) "Mechanisms and models of narrow-V wakes," ORI Technical Report 2529 of 30 October.

Table 1--Summary of Photographic Collection

Fig.	Mission	Roll	Frame	Location	Land Feature	Photo Ctr. Coordinates	Sol. Ele.	Alt.	Cam. Type	Focal Length
6	41-B	33	1431	Pacific	--	--	--	--	Has.	100mm
7			1432	Pacific	--	--	--	--	Has.	100
8			1433	Pacific	--	--	--	--	Has.	100
9	41-C	31	1009	G. Oman	Oman	24.0N 57.5E	--	--	Has.	250
10	41-G	35	71	Arabian S.	Al Masirah	20.5N 59.0E	39°	140nm	Has.	250
11			72	Arabian S.	Al Masirah	20.5N 59.0E	39	140	Has.	250
12			87	Mediter. S.	--	34.0N 21.0E	39	128	Has.	250
13		38	43	Iran	Sir Bu Nuahi	25.5N 54.0E	44	122	Has.	250
14			55	Ionian S.	--	37.0N 21.0E	41	123	Has.	250
15			59	Ionian S.	--	35.5N 21.5E	42	123	Has.	250
16			60	Ionian S.	--	35.5N 22.0E	42	123	Has.	250
17			61	Mediter. S.	--	35.3N 25.3E	42	123	Has.	250
18			62	Mediter. S.	Libya	32.5N 24.5E	42	123	Has.	250
19			63	Mediter. S.	--	32.5N 25.0E	43	123	Has.	250
20			64	Mediter. S.	--	32.5N 25.0E	43	122	Has.	250
21			80	Mediter. S.	--	38.5N 1.5W	41	136	Has.	250
22			81	Mediter. S.	--	38.5N 1.0W	41	136	Has.	250
23		39	71	N.Y. Bight	L. Island	41.0N 73.0W	38	124	Has.	100
24			72	N.Y. Bight	L. Island	41.0N 73.0W	38	124	Has.	100
25		42	54	Mediter. S.	Libya	33.5N 24.0E	42	123	Has.	50
26			55	Mediter. S.	Libya	33.5N 24.0E	42	123	Has.	50
27			56	Mediter. S.	Libya	33.5N 24.0E	42	123	Has.	50
28		43	50	English Ch.	Dover-Calais	51.0N 1.5E	31	125	Has.	250
29	61-A	34	15	G. Mexico	--	22.7N 94.5W	51	177	Has.	250
30		200	44	G. Crete	Crete	35.5N 25.0E	37	175	Lin.	250
31		200	45	G. Crete	Crete	35.0N 26.0E	36	175	Lin.	250
32		200	46	G. Crete	Crete	35.5N 26.0E	36	175	Lin.	250
33		200	47	G. Crete	Crete	35.5N 26.5E	36	175	Lin.	250
34		200	48	G. Crete	Crete	35.5N 27.0E	35	175	Lin.	250

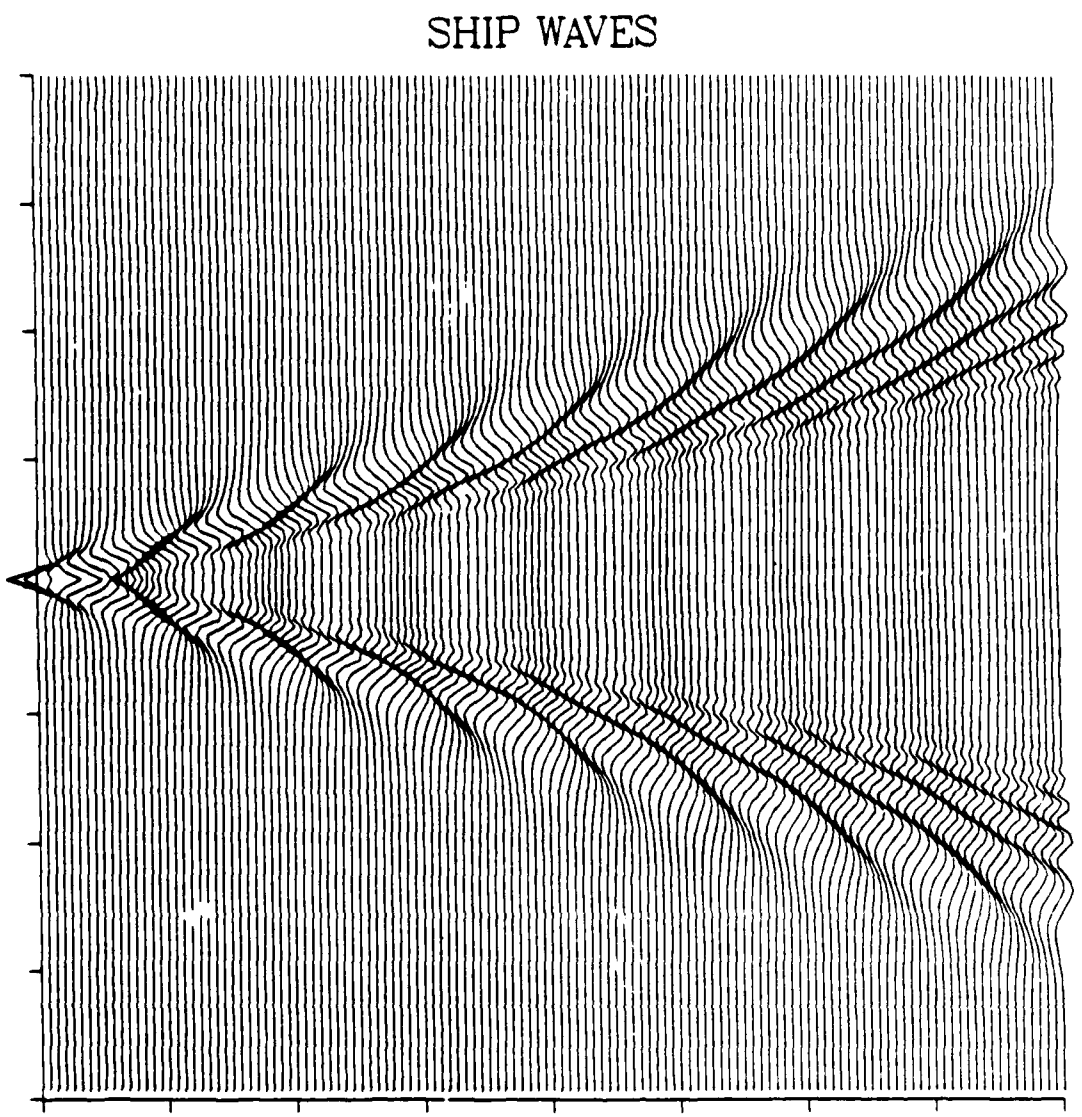

Figure 1. Kelvin waves from a moving ship. Calculations employ the ORI Kelvin Waves Code.

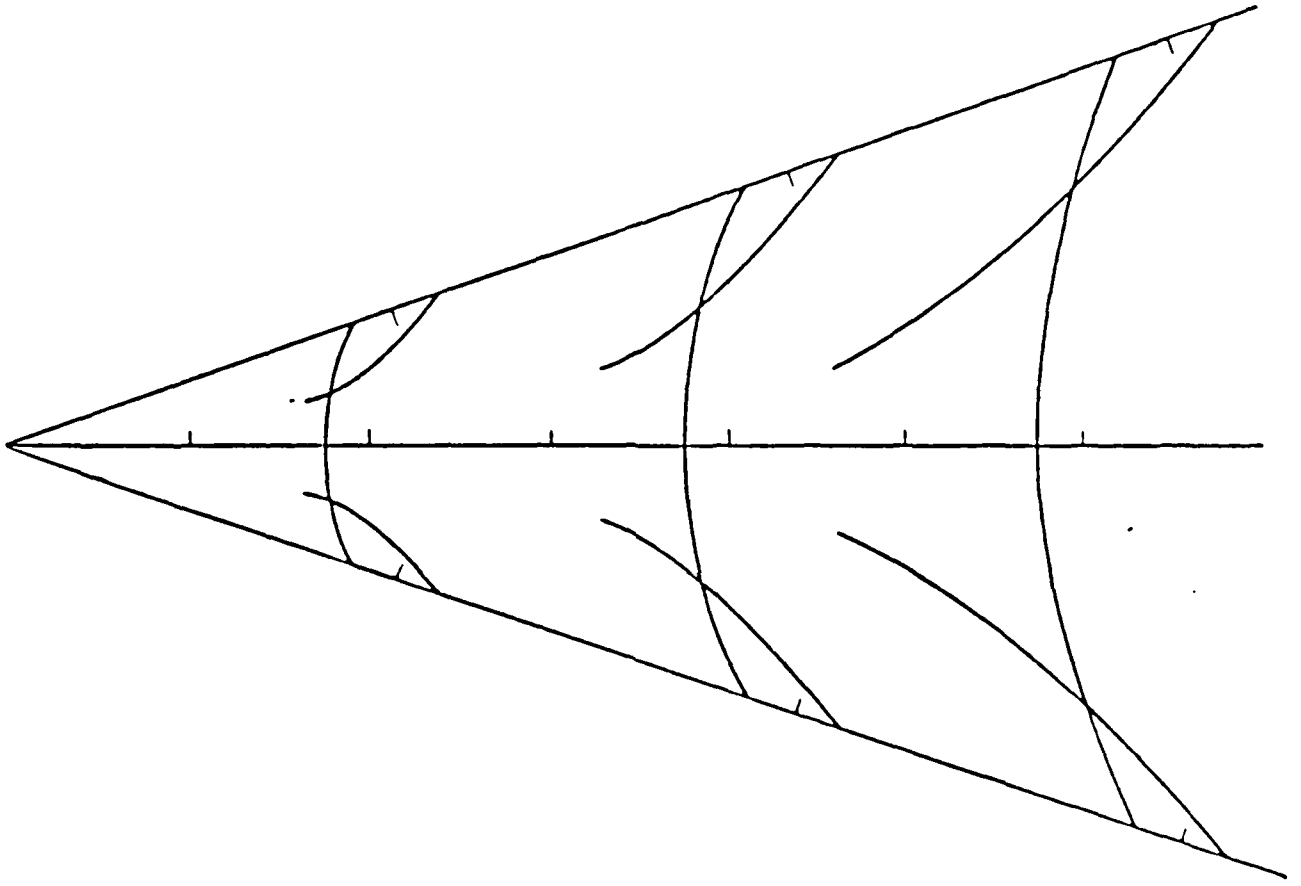

Figure 2. Crests of Kelvin waves. Taken from Wehausen and Laitone (1960).

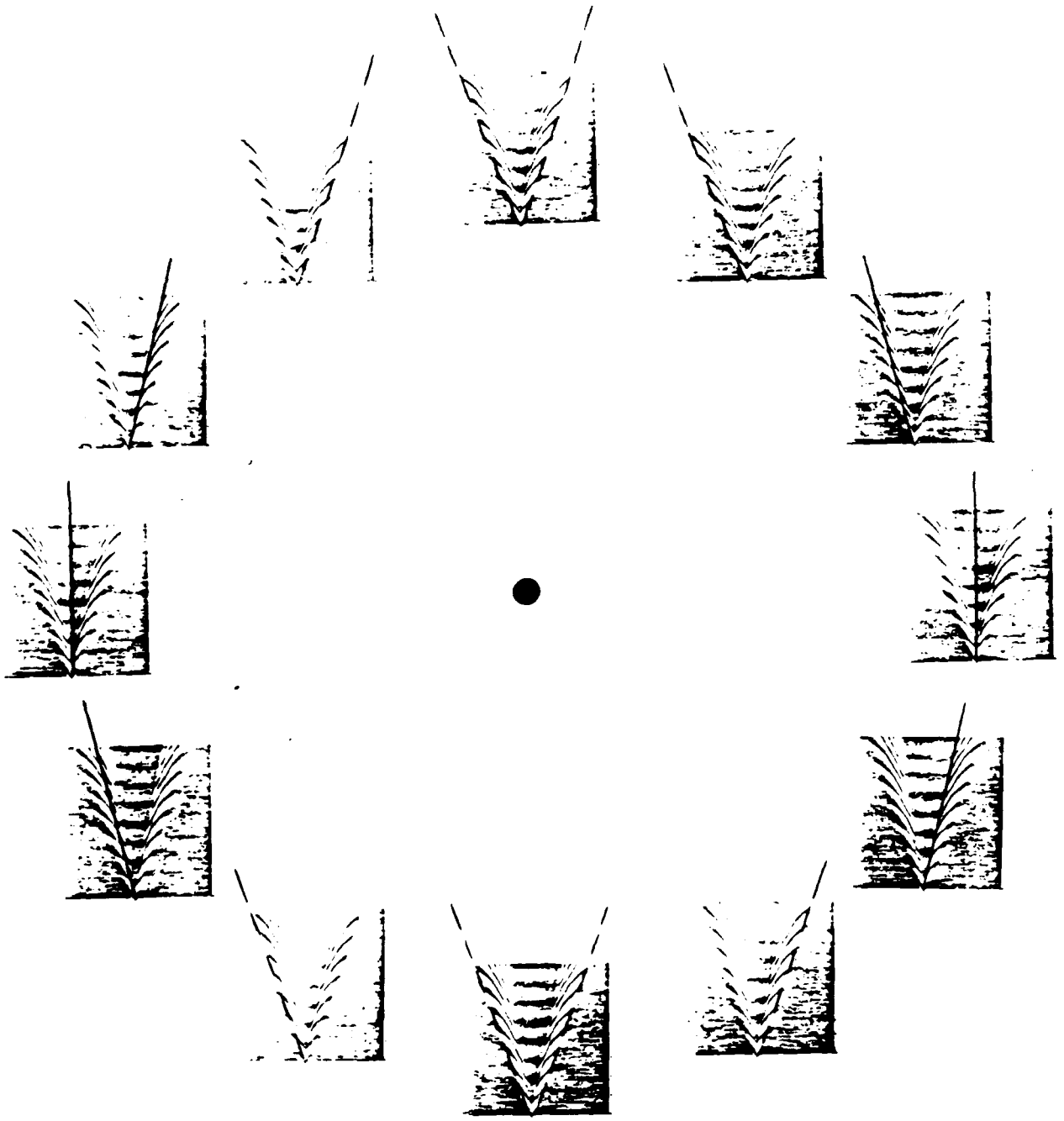

Figure 3. Geometrical influence of Kelvin-wave optical imaging. The solar reflection point is at the center. Solid lines indicate where divergent waves face the solar point. Dashed lines indicate which arm(s) would be better imaged when none of the divergent waves face the solar point directly.

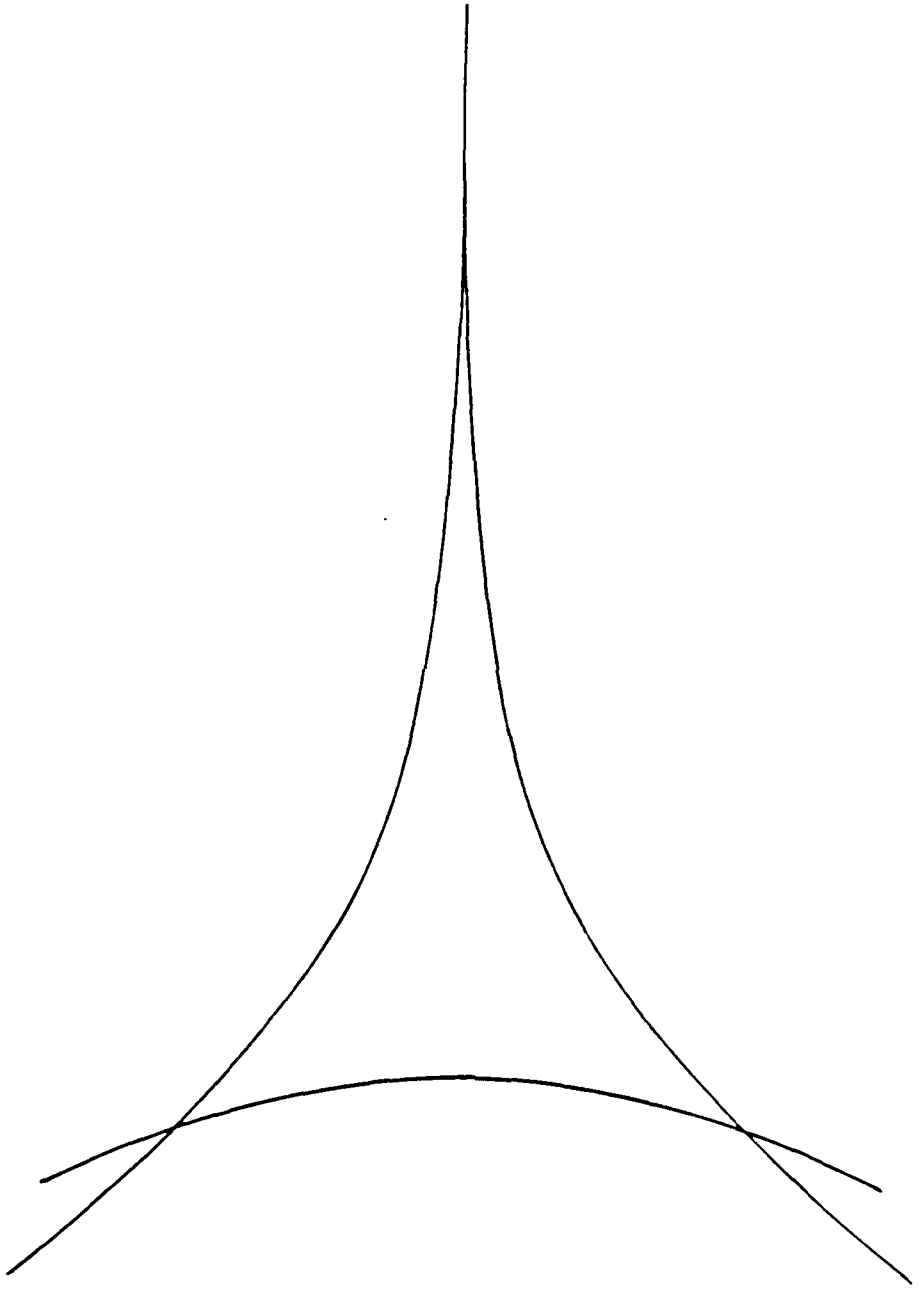

Figure 4. A single pair of Kelvin divergent-wave crests and the single transverse-wave crest that is nearest them at the cusps.

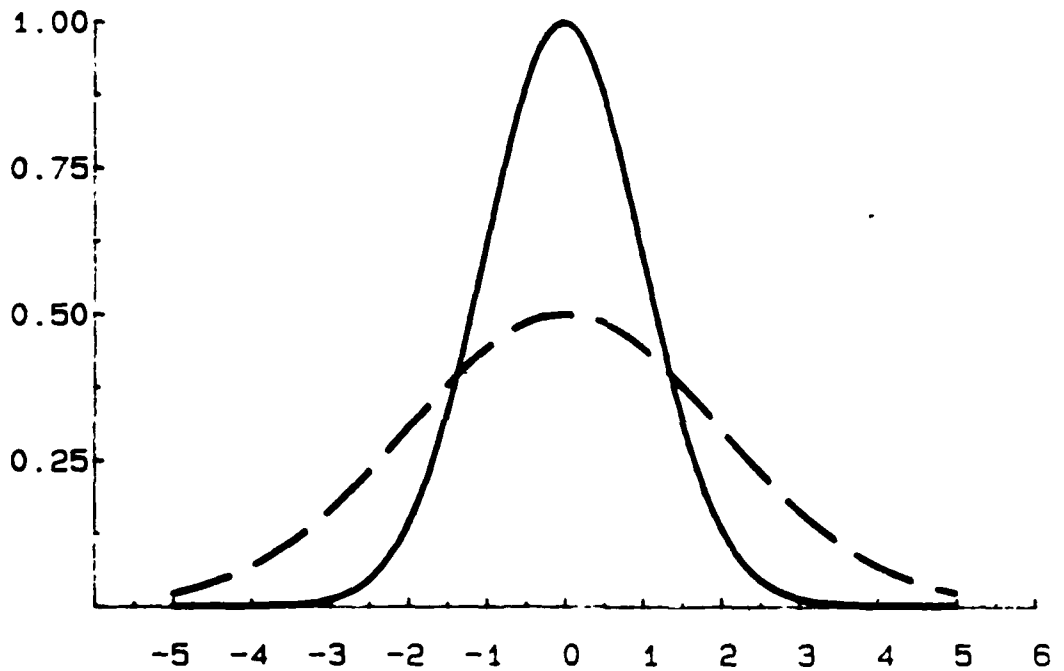

Figure 5. Light intensity from the sea surface through a glitter pattern. Solid curve - relatively calm ocean surface. Dashed curve - relatively rough ocean surface.

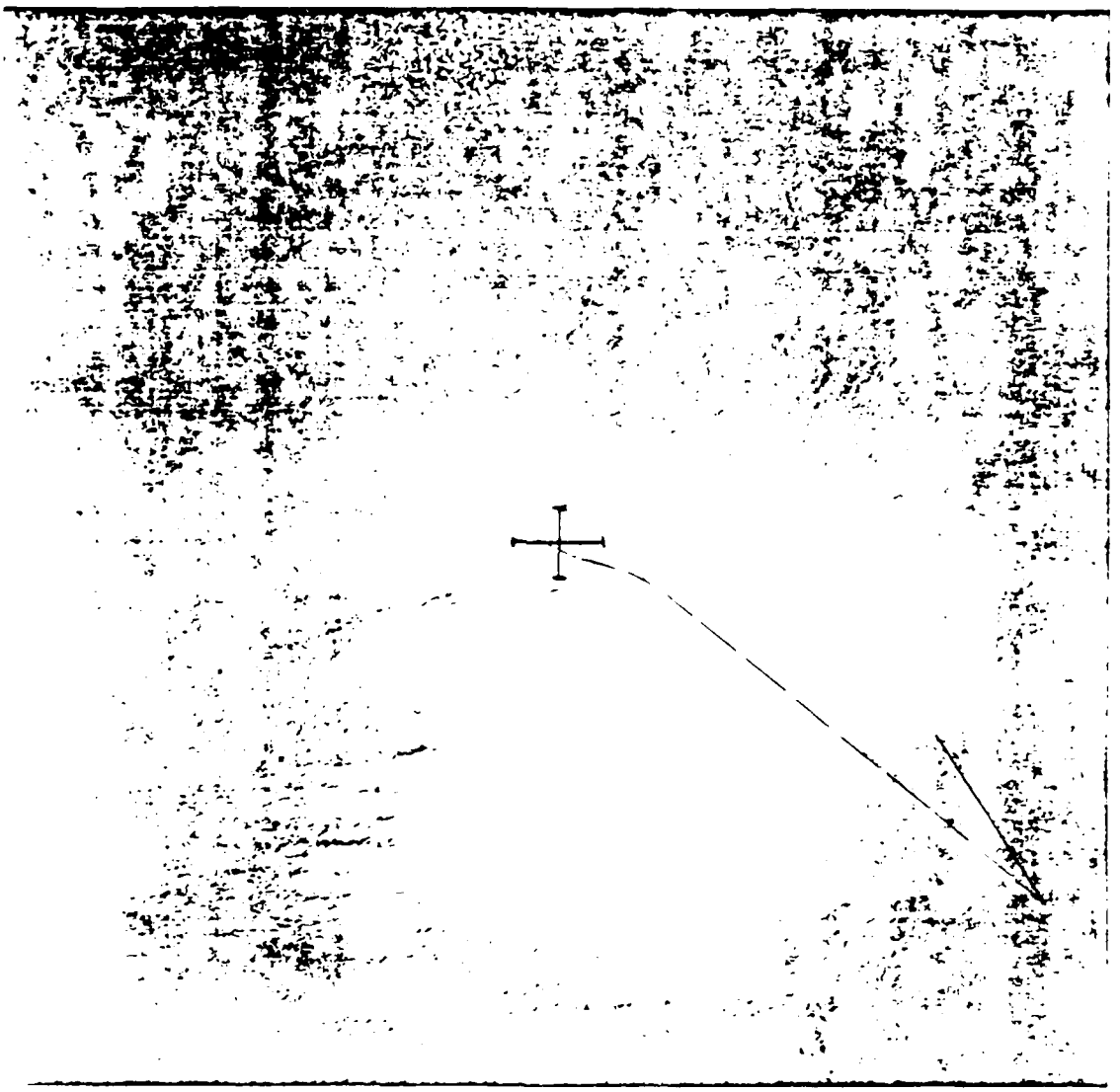

Figure 6. Photograph 41-B 33 1431

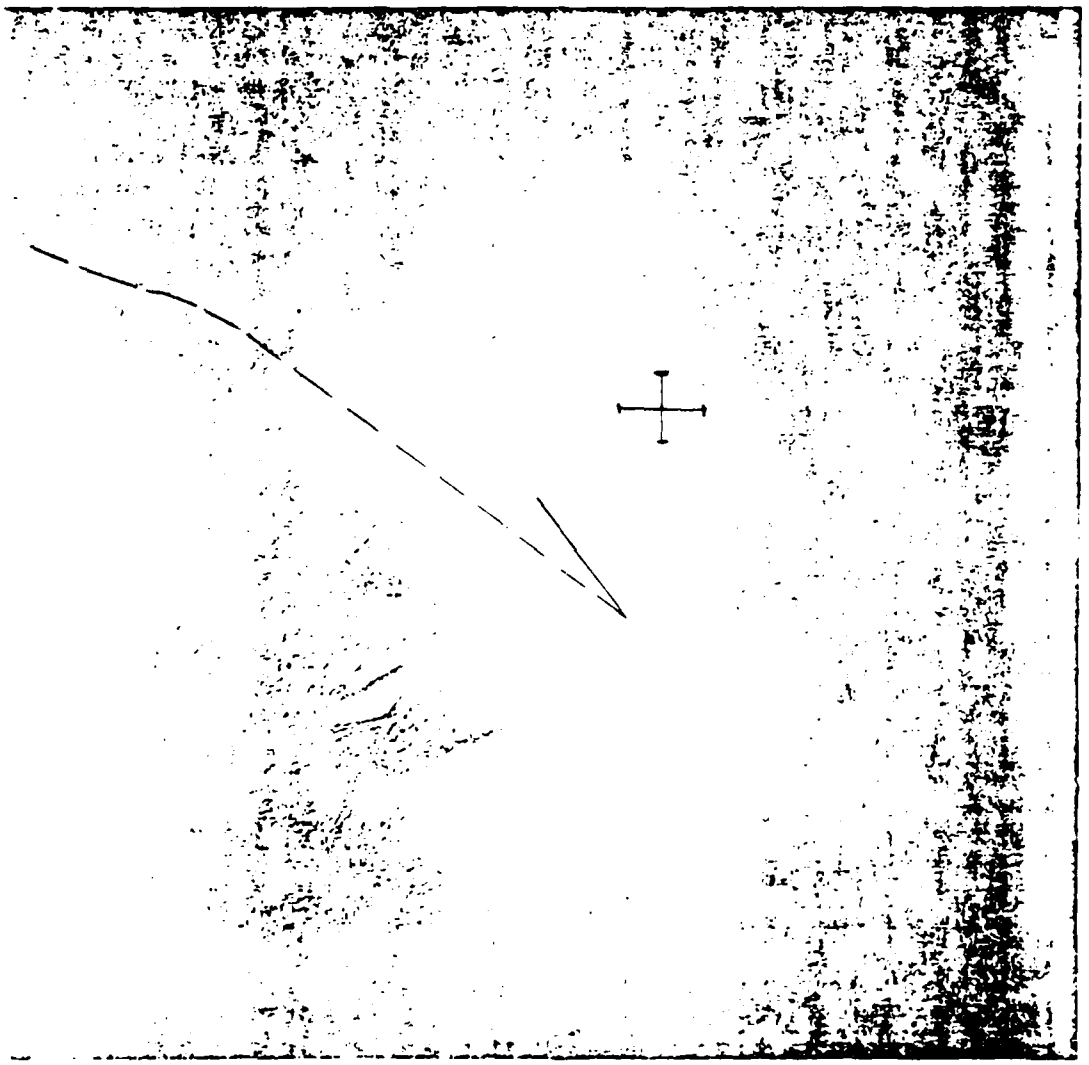

Figure 7. Photograph 41-B 33 1432

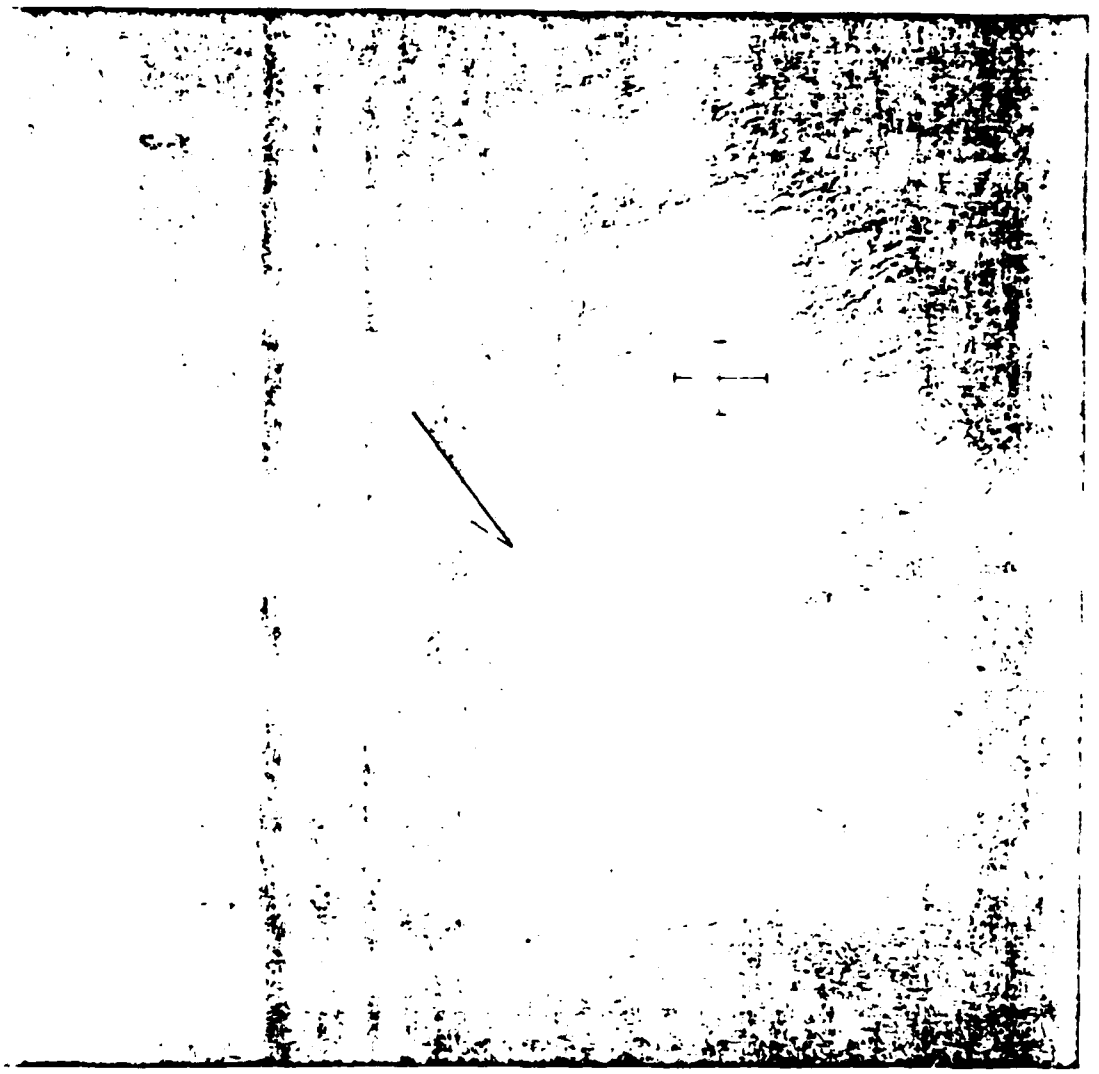

Figure 8. Photograph 41-B 33 1433

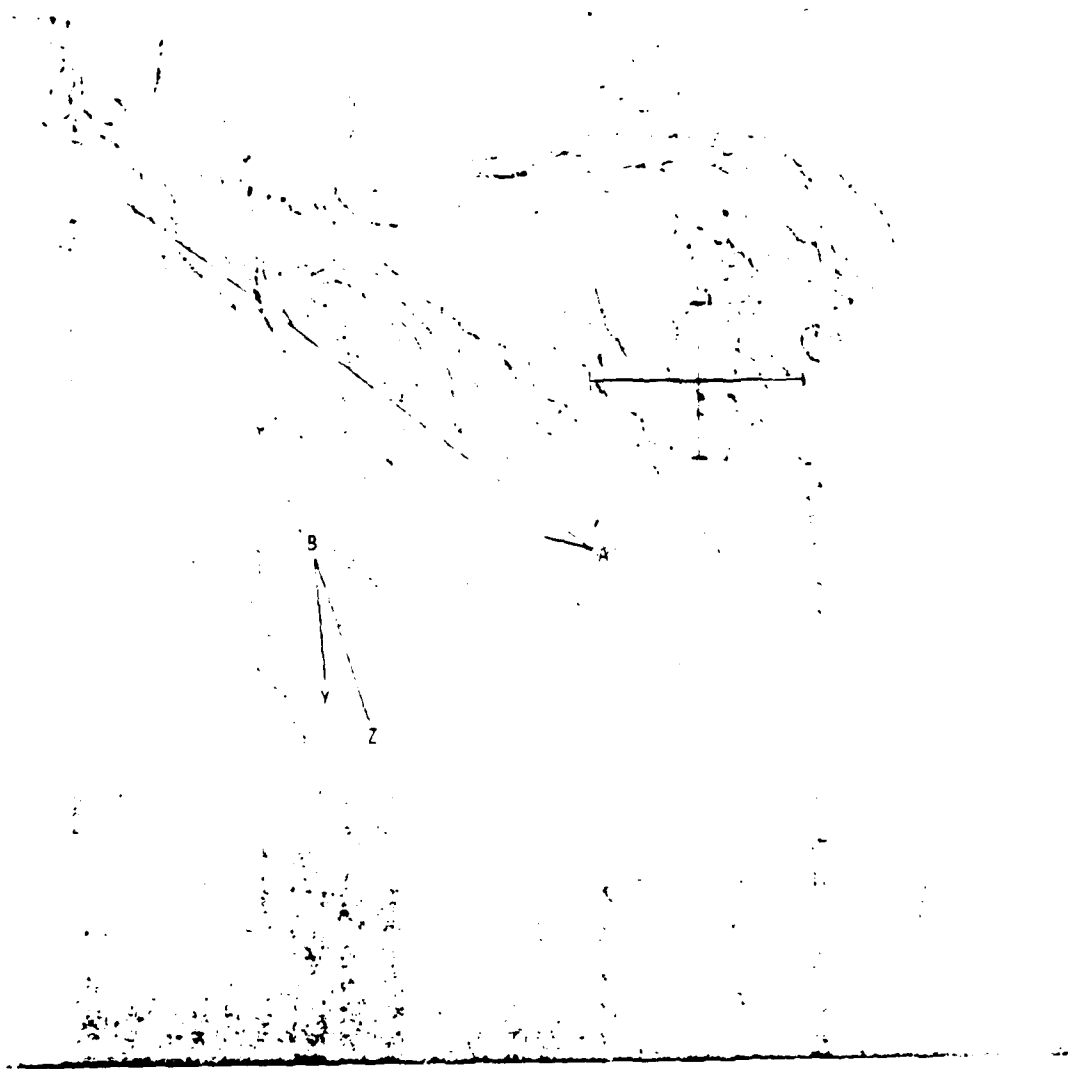

Figure 9. Photograph 41-C 31 1009

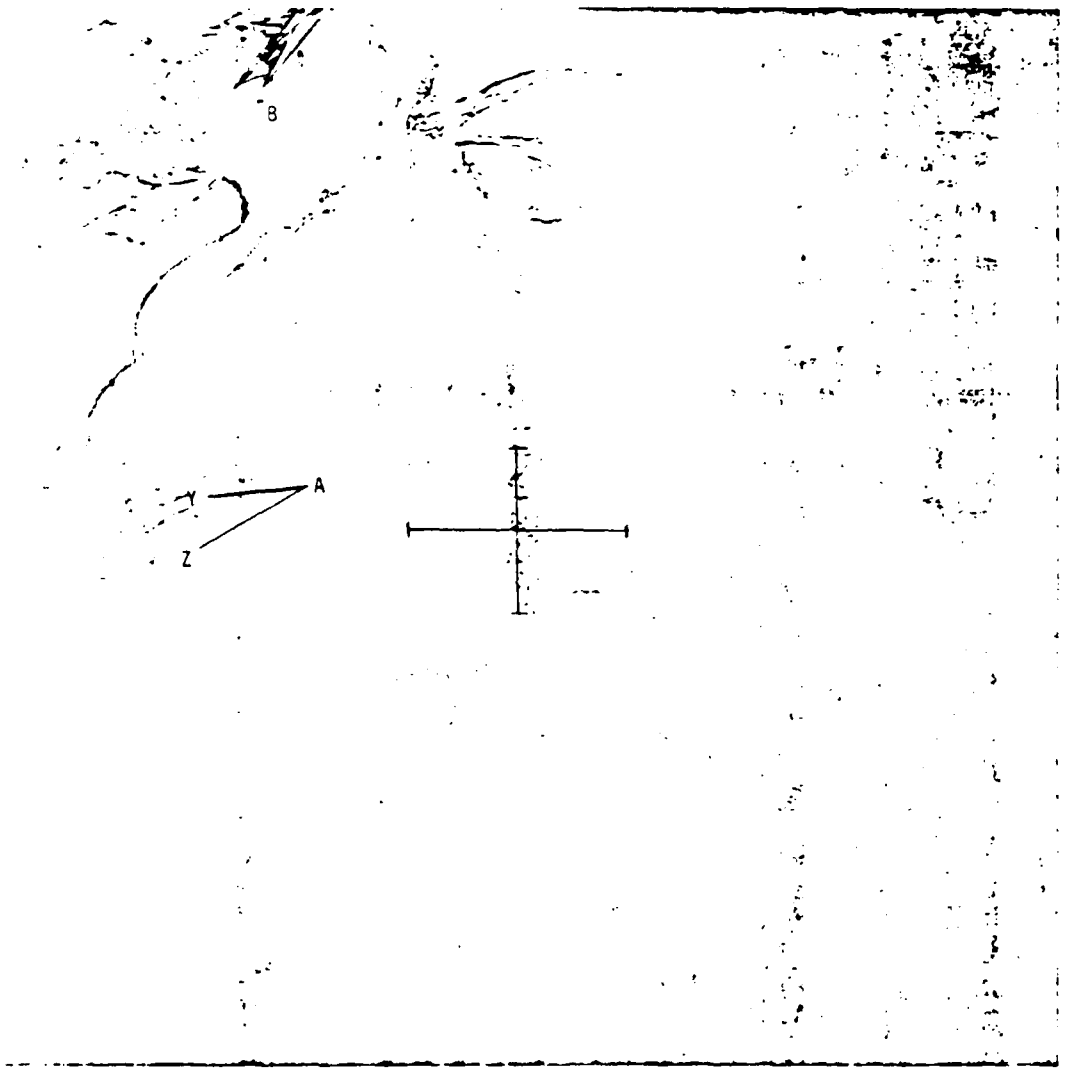

Figure 10. Photograph 41-G 35 71

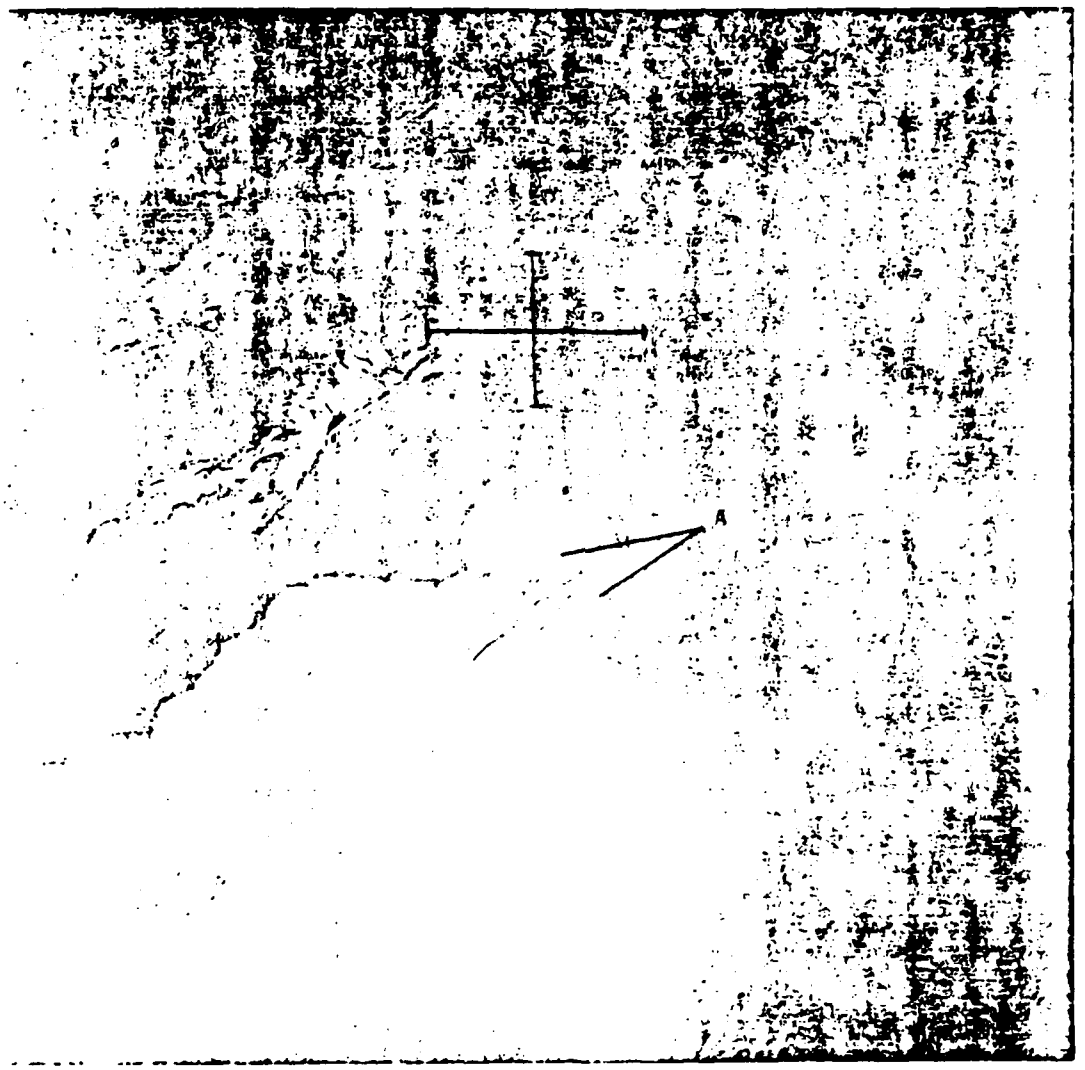

Figure 11. Photograph 41-G 35 72

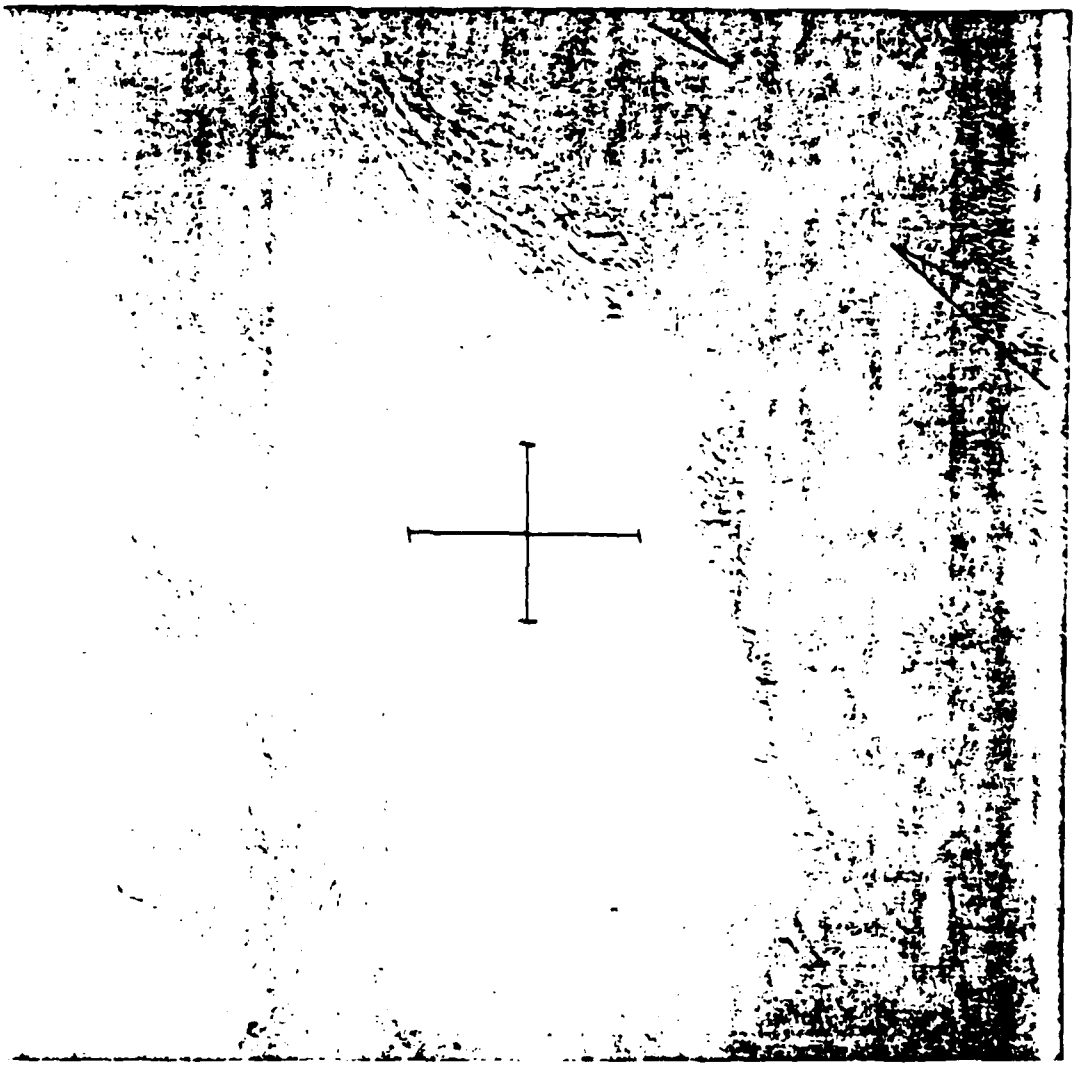

Figure 12. Photograph 41-G 35 87

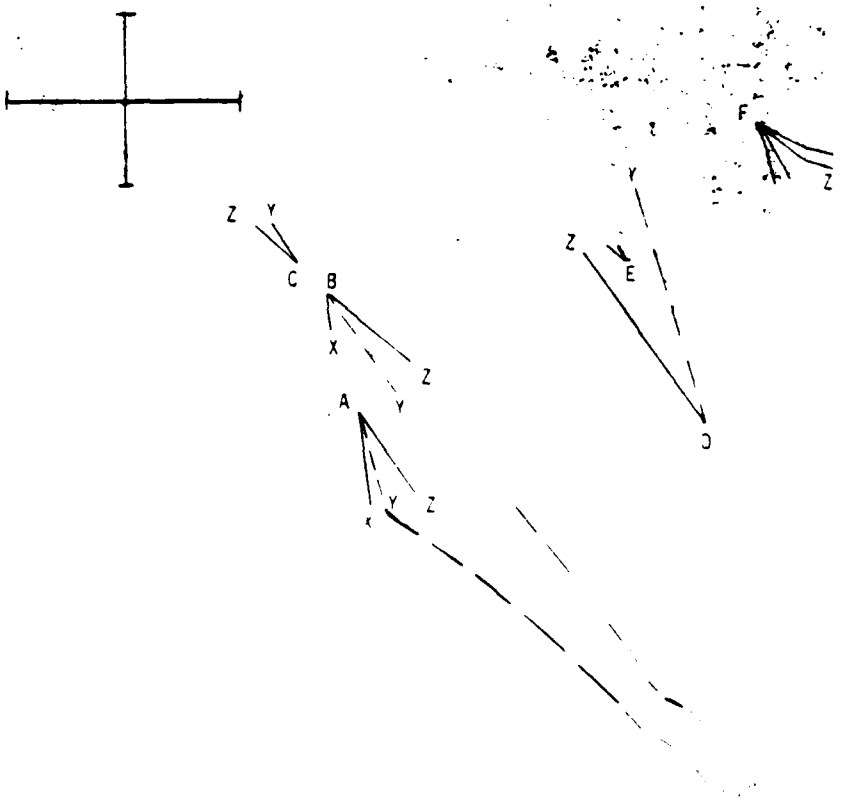

Figure 13. Photograph 41-G 38 43

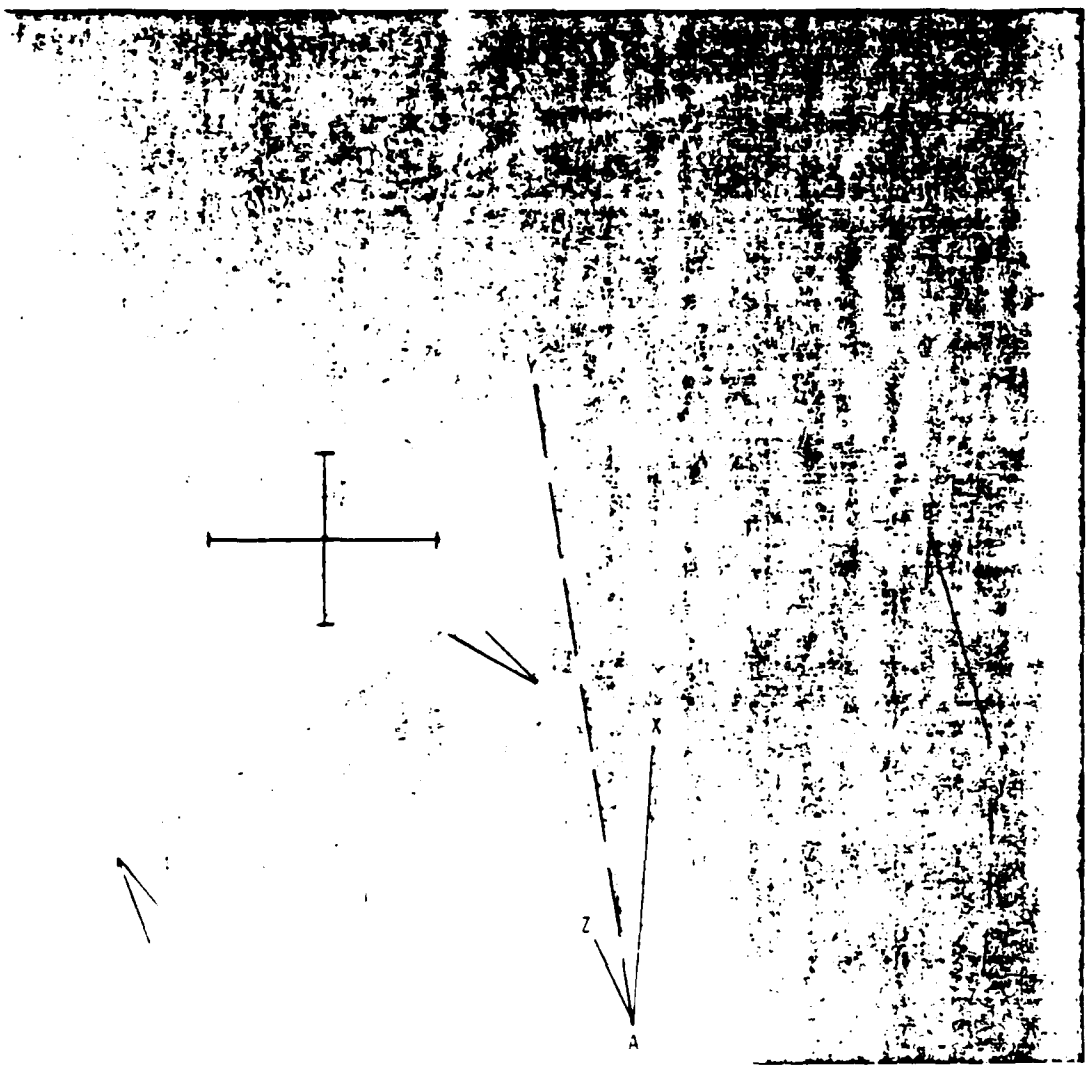

Figure 14. Photograph 41-G 38 55

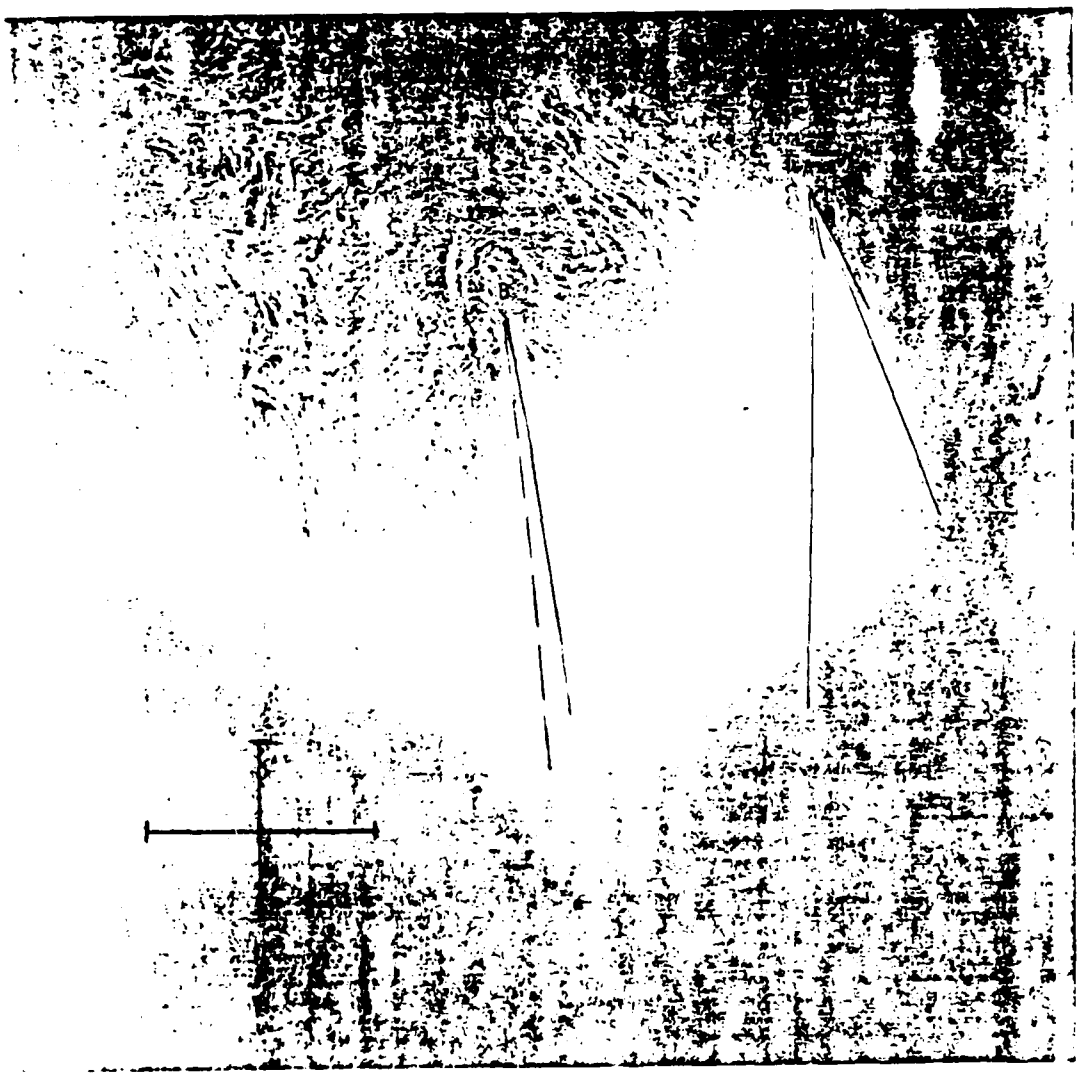

Figure 15. Photograph 41-G 38 59

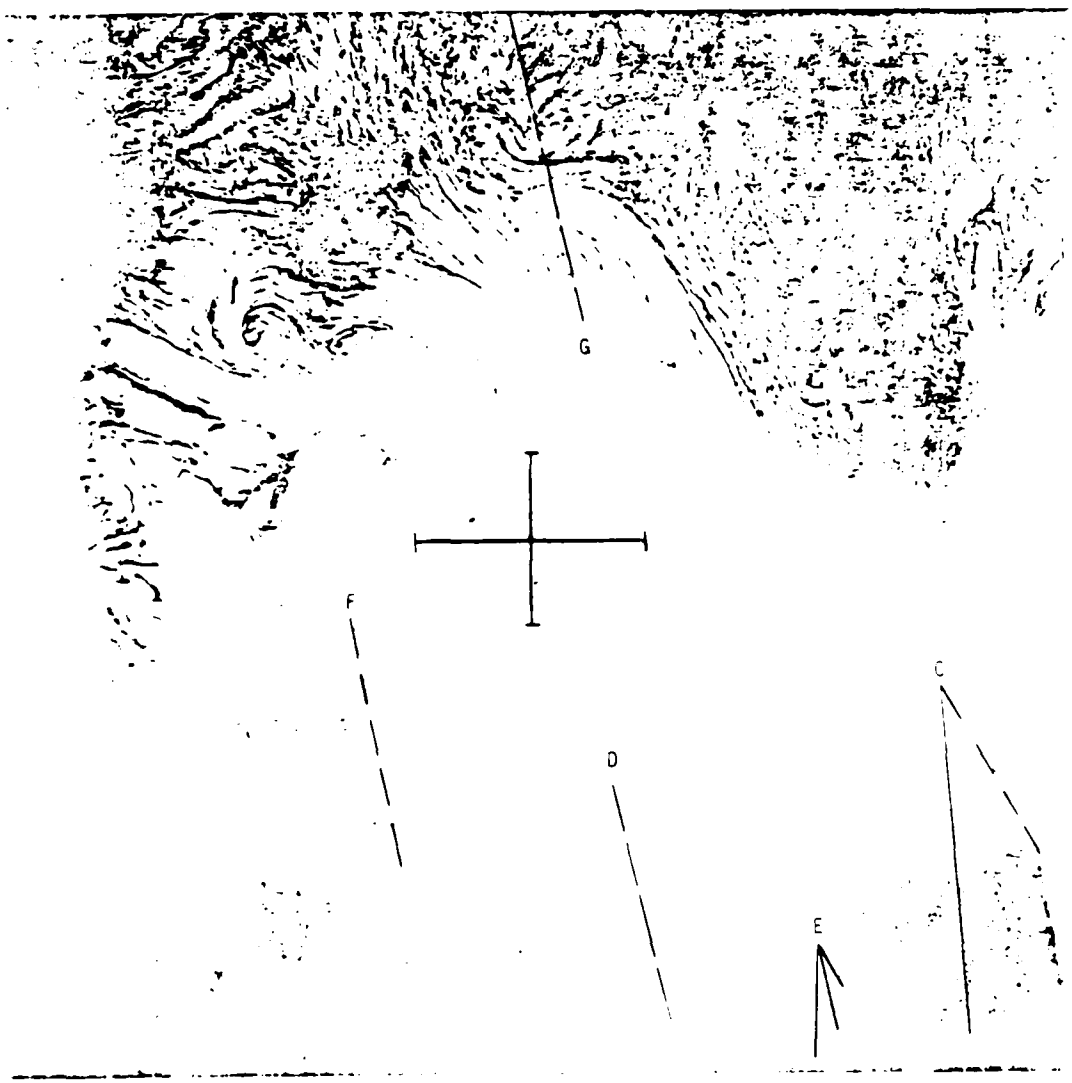

Figure 16. Photograph 41-G 38 60

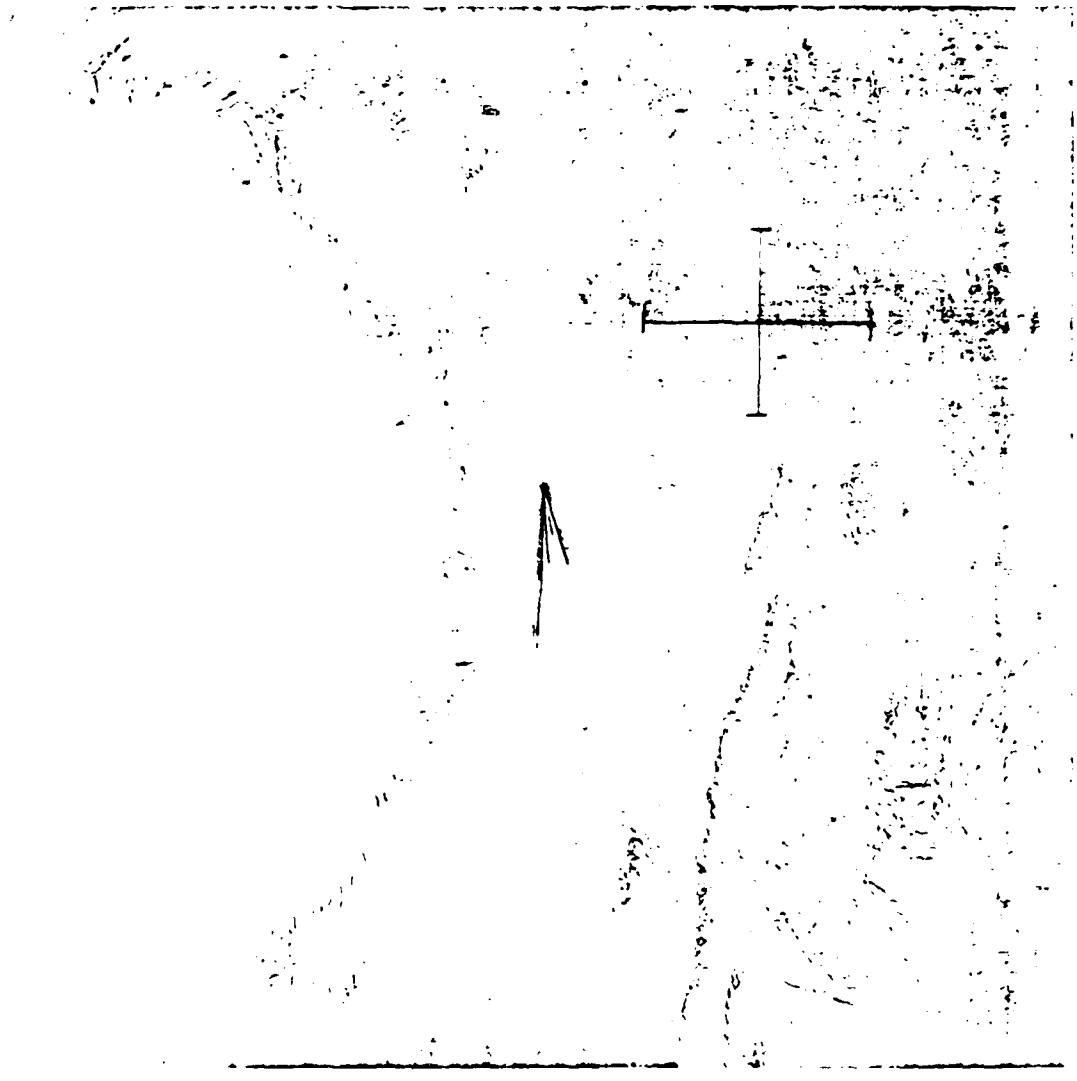

Figure 17. Photograph 41-G 38 61

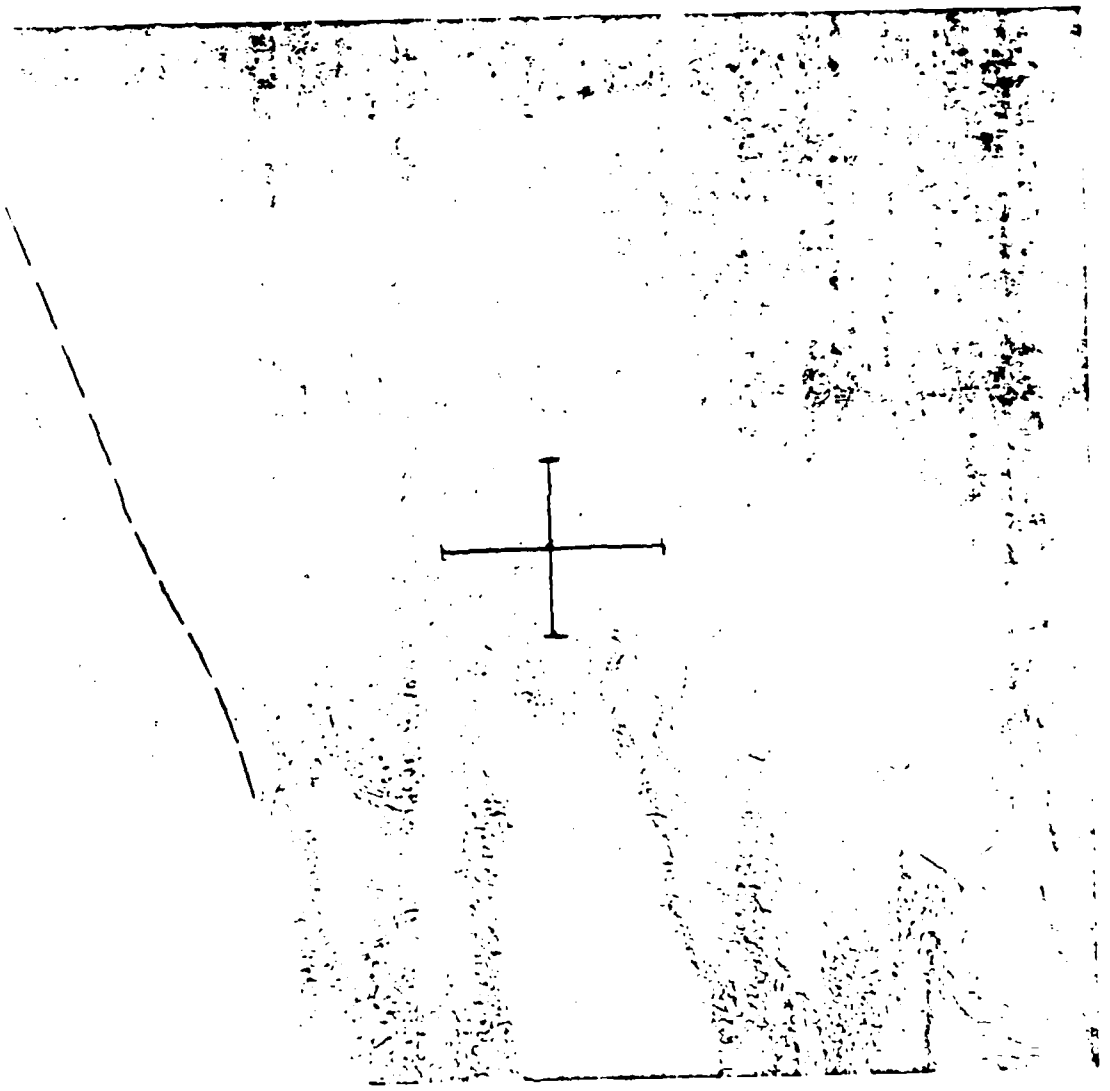

Figure 18. Photograph 41-G 38 62

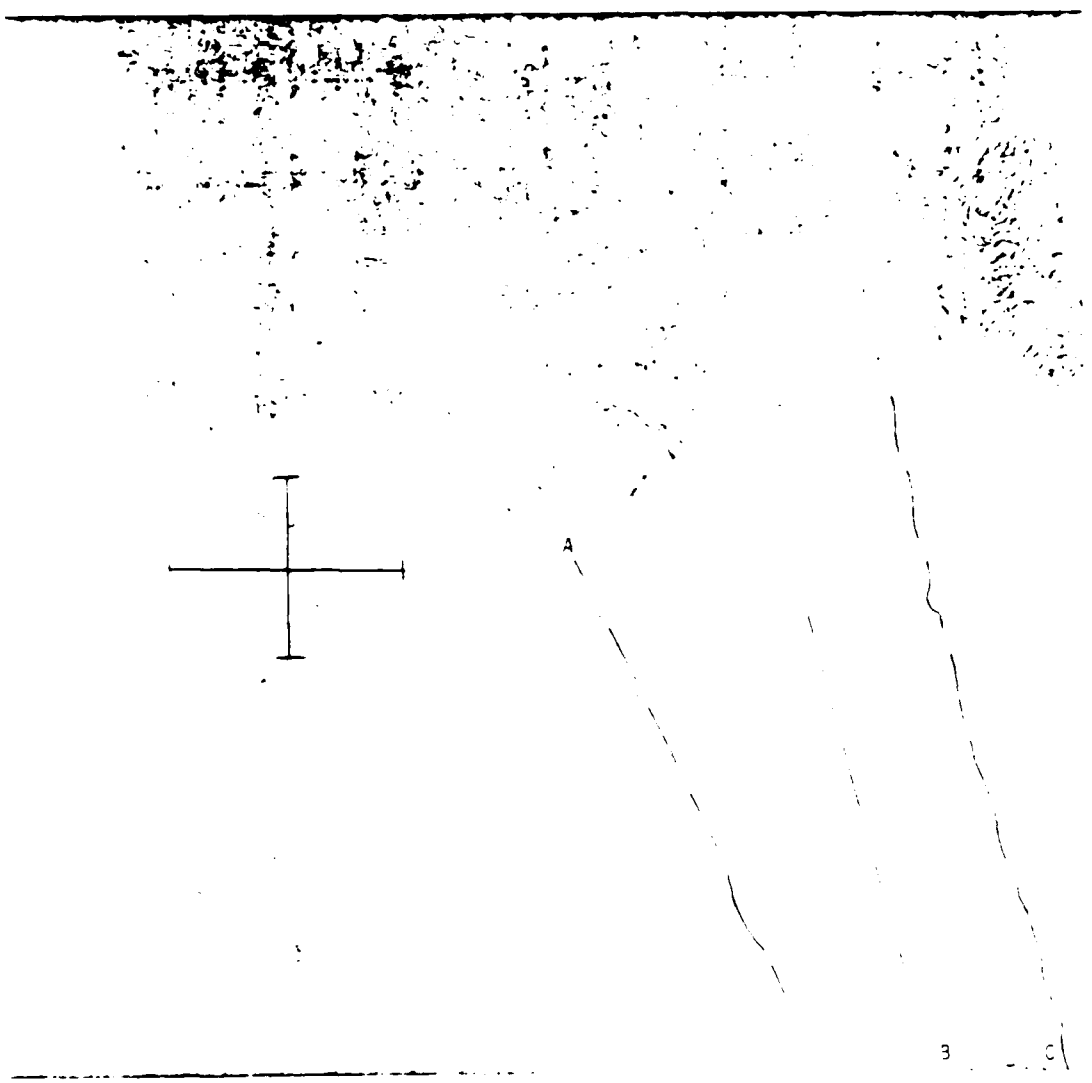

Figure 19. Photograph 41-G 38 63

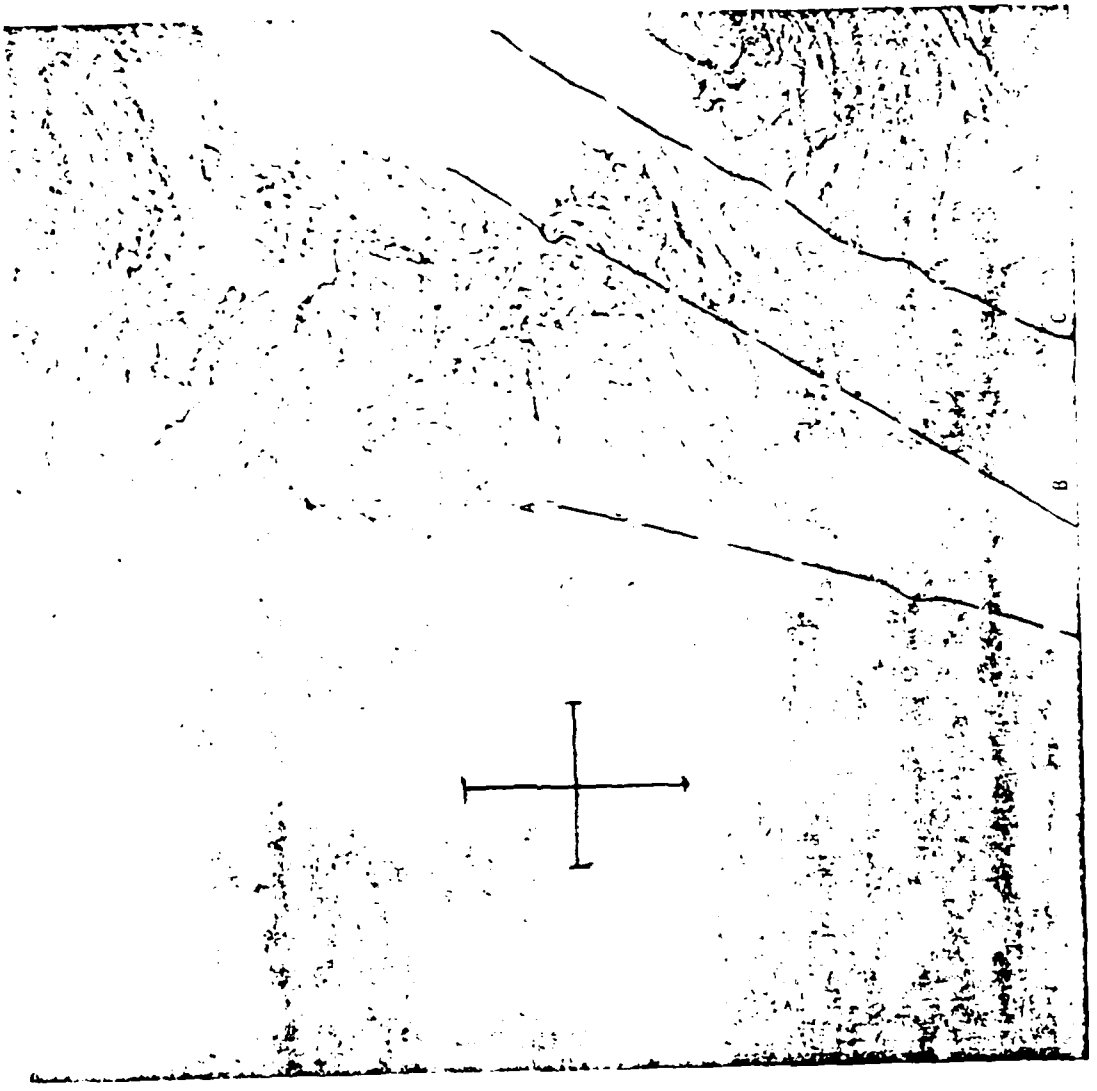

Figure 20. Photograph 41-G 38 64

Figure 21. Photograph 41-G 38 80

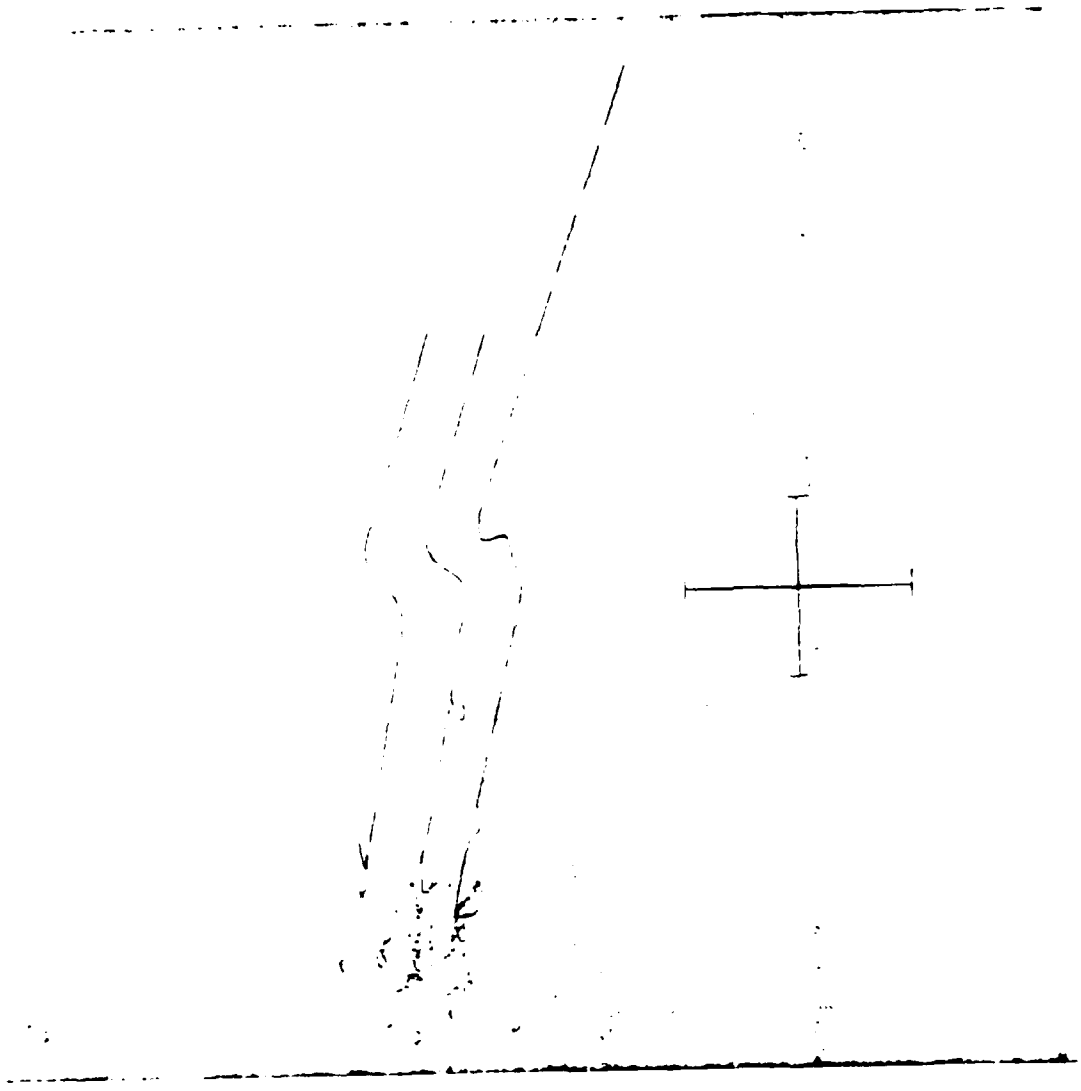

Figure 22 Photograph 41-G-38-81

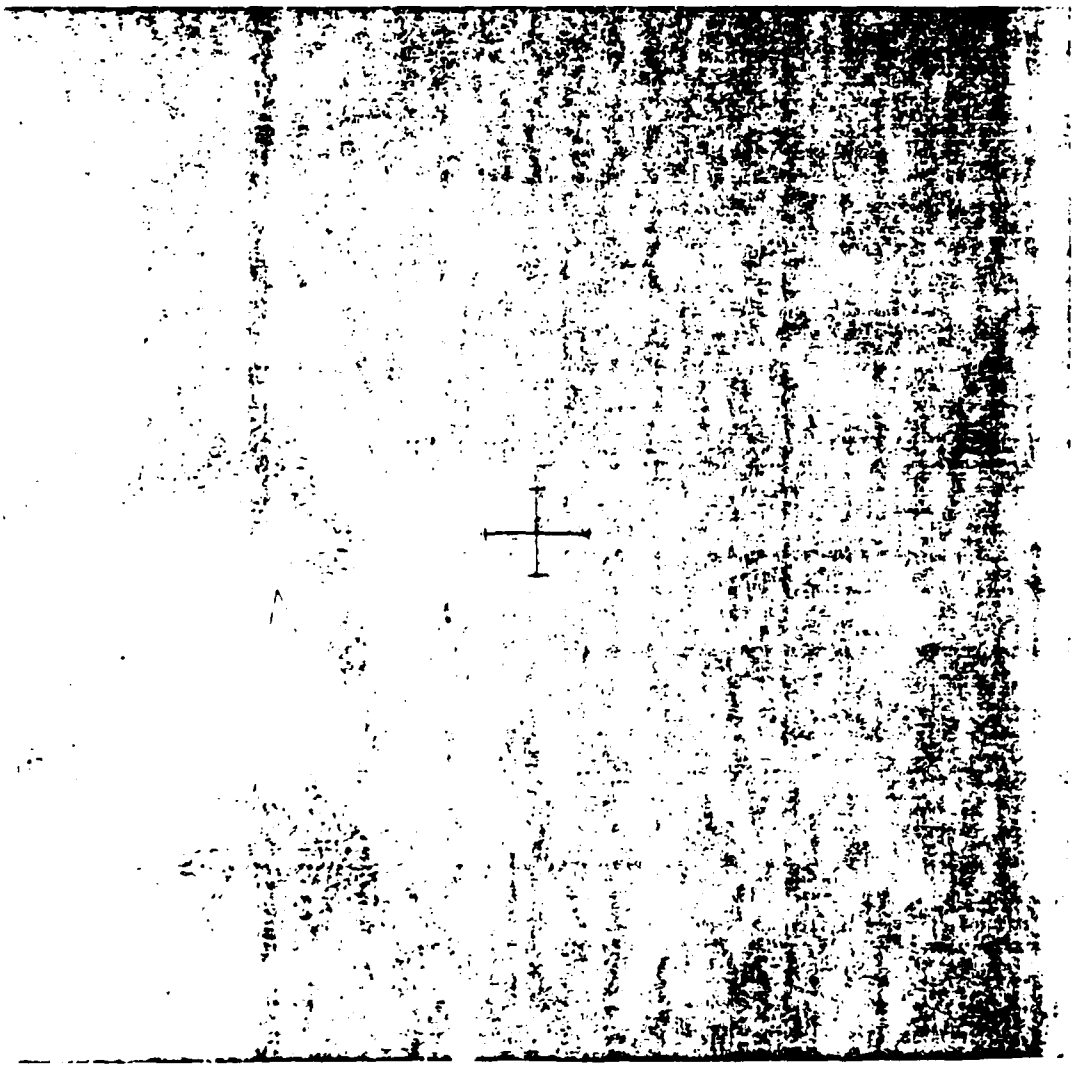

Figure 23. Photograph 41-G 39 71

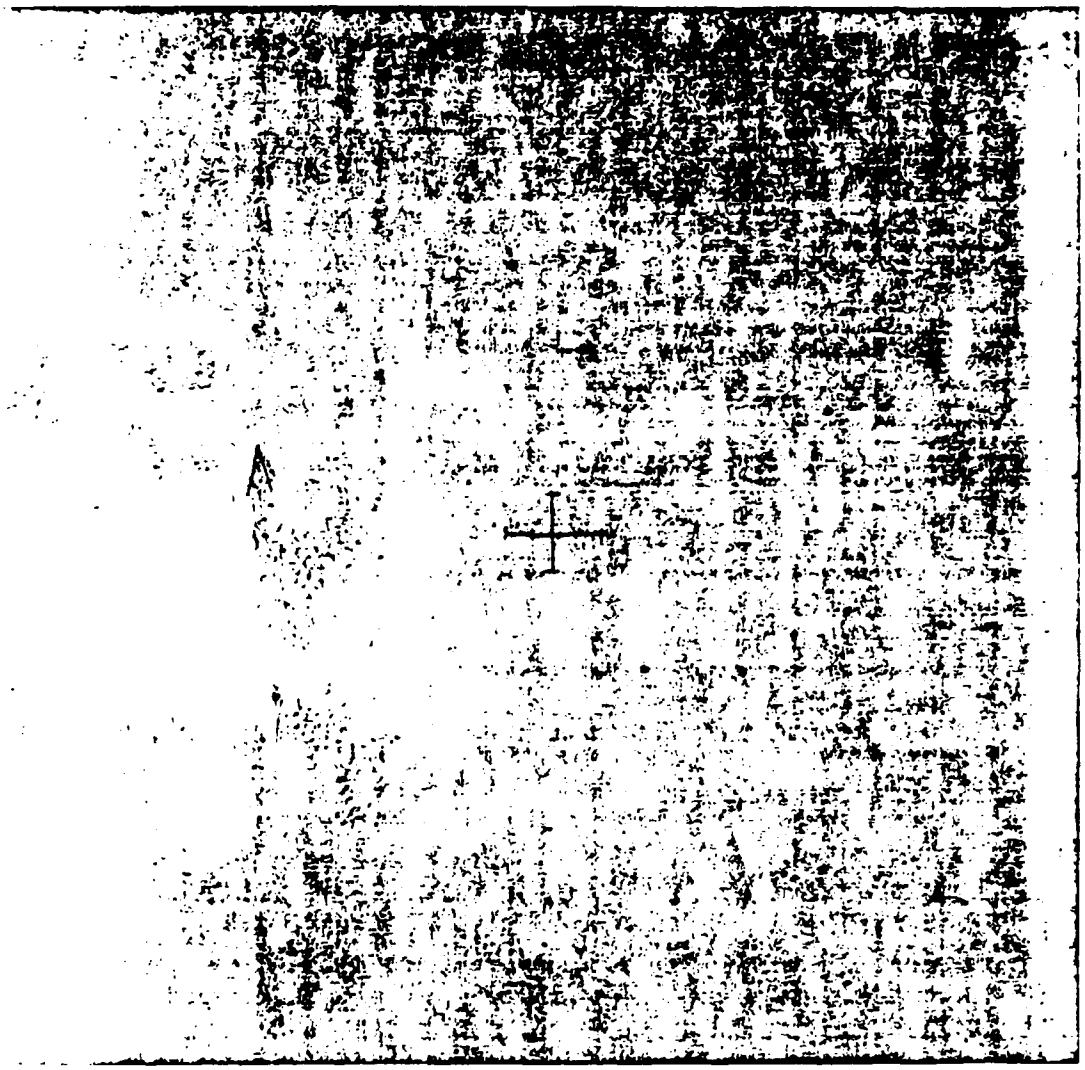

Figure 24. Photograph 41-G 39 72

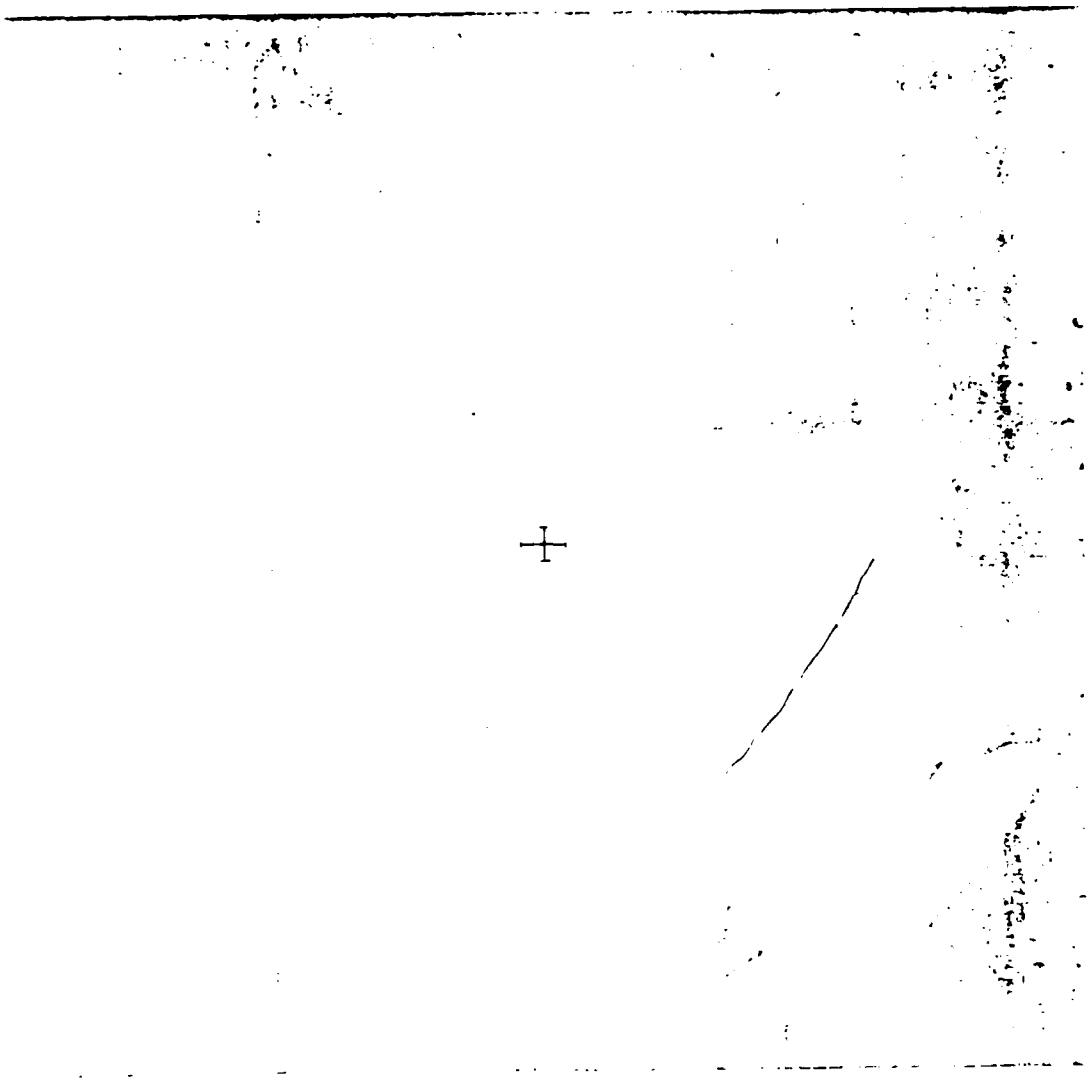

Figure 25. Photograph 41-G 42 54

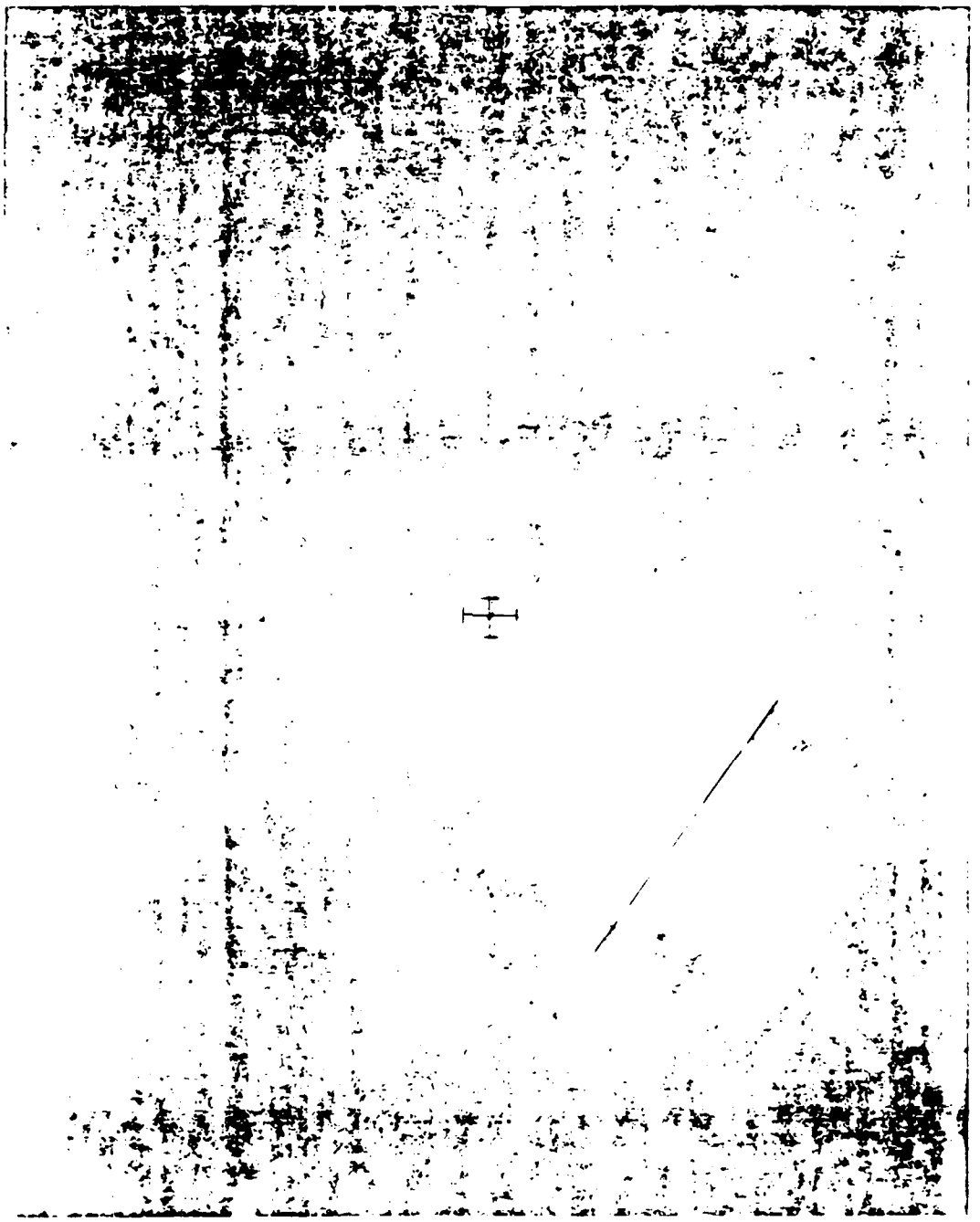

Figure 26. Photograph 41-G 42 55

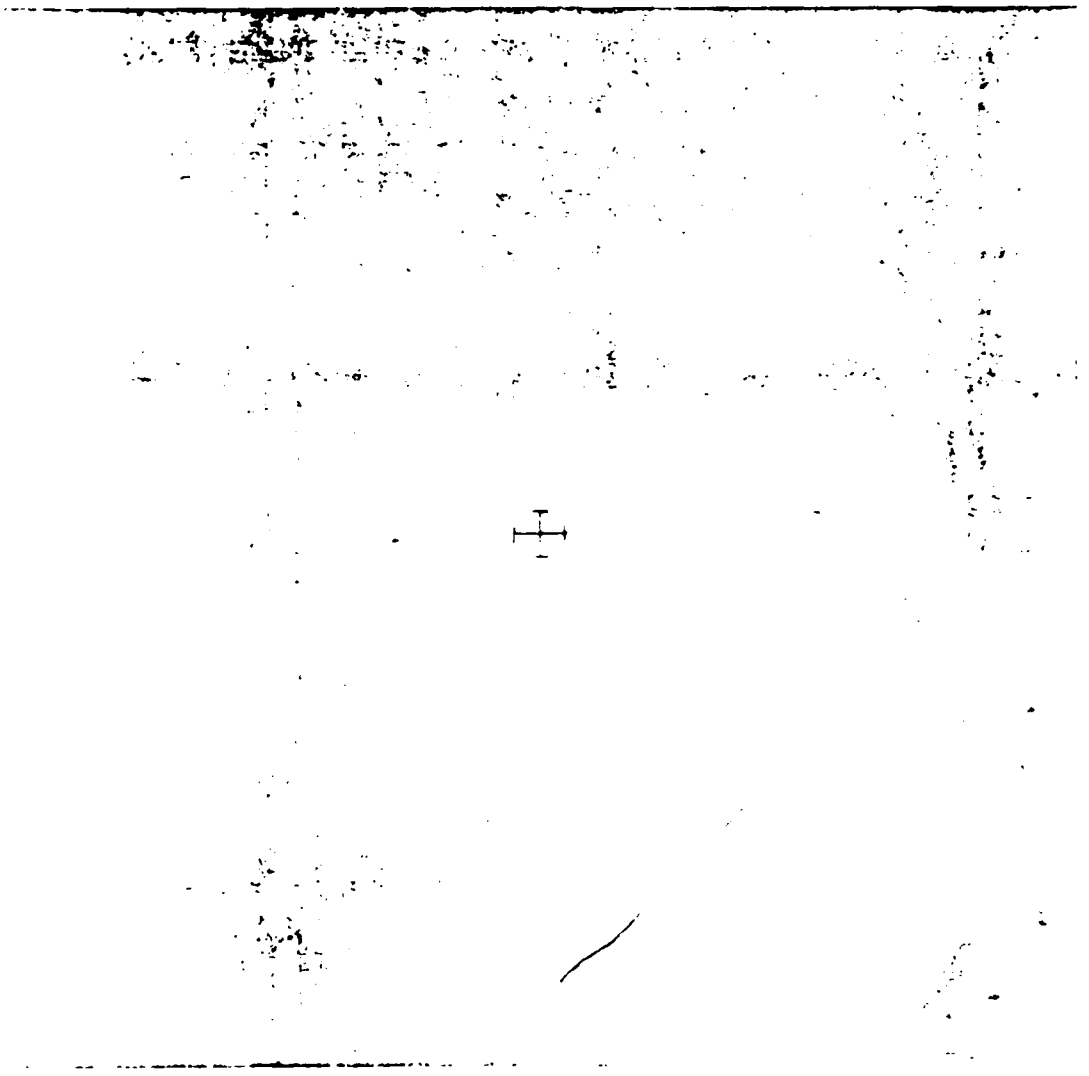

Figure 27. Photograph 41-G 42 56

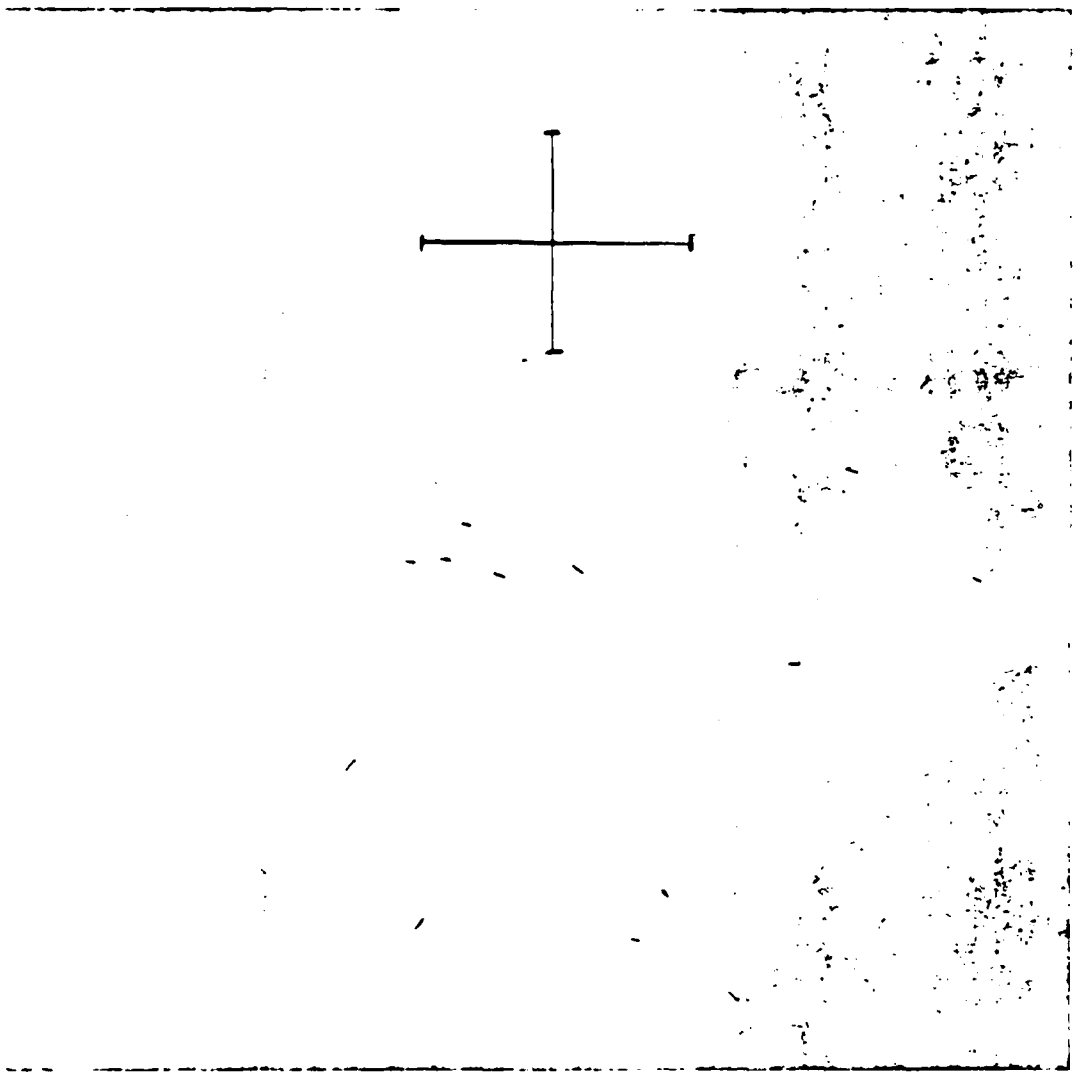

Figure 28. Photograph 41-G 43 50

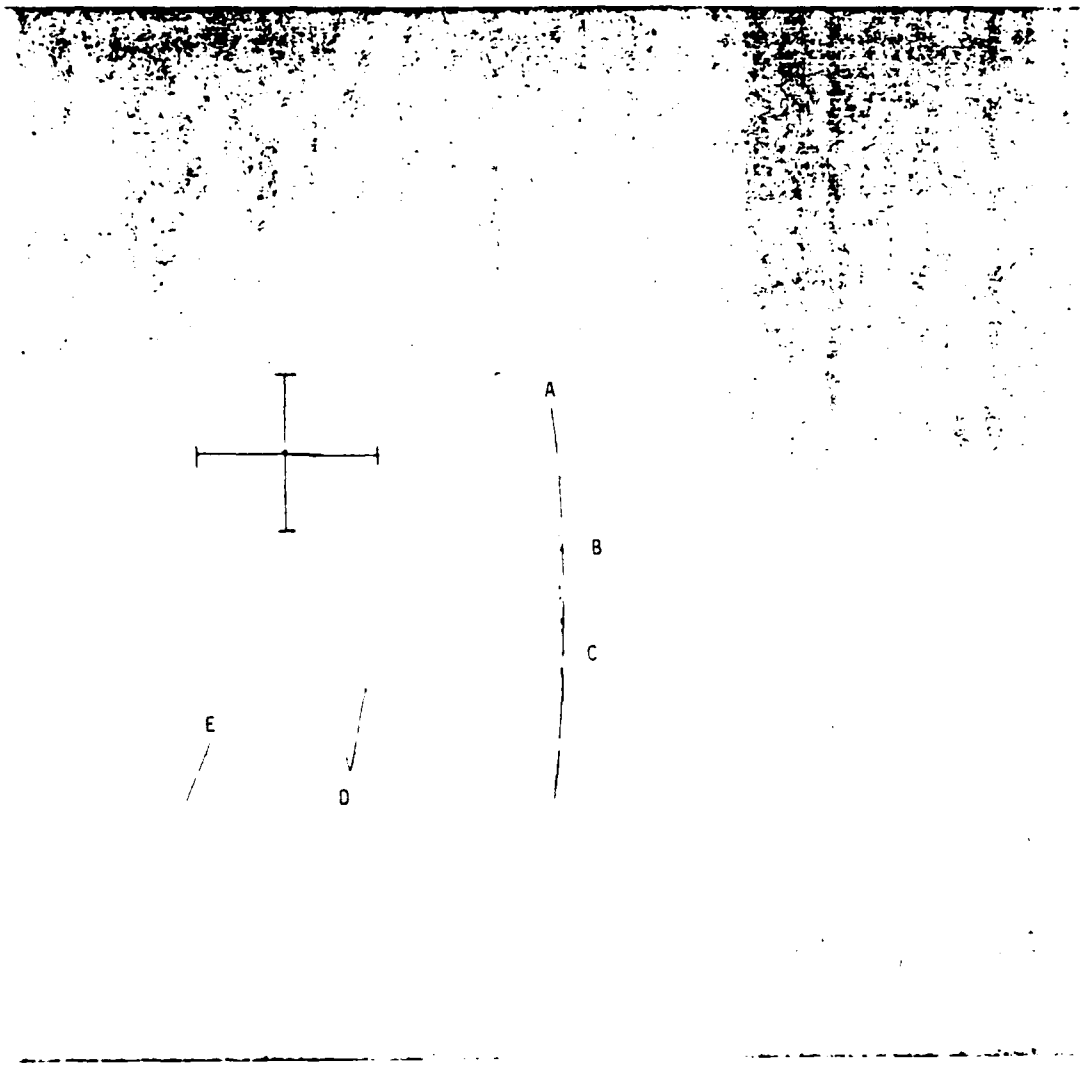

Figure 29. Photograph 61-A 34 15

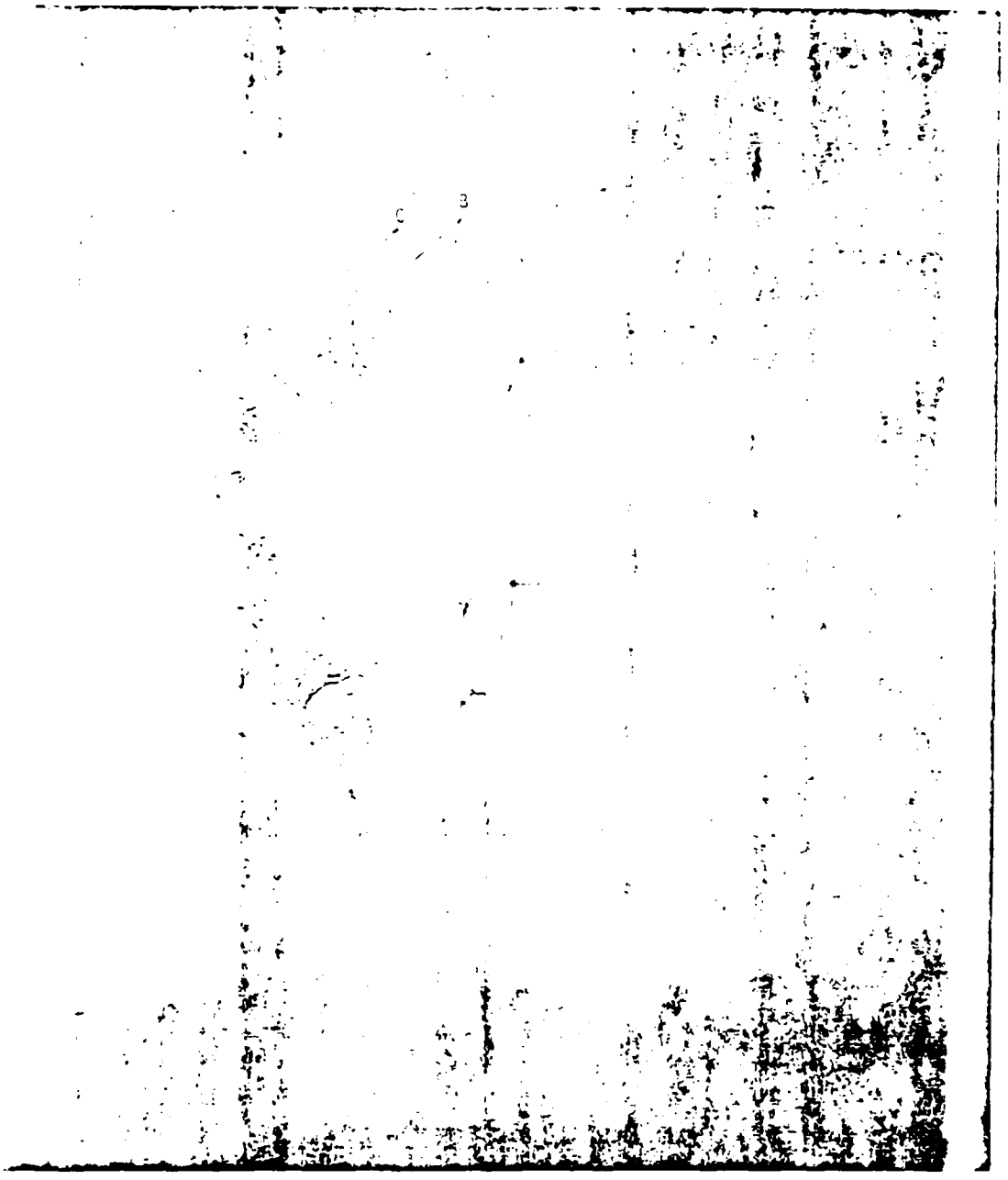

Figure 30. Photograph 61-A 200 44

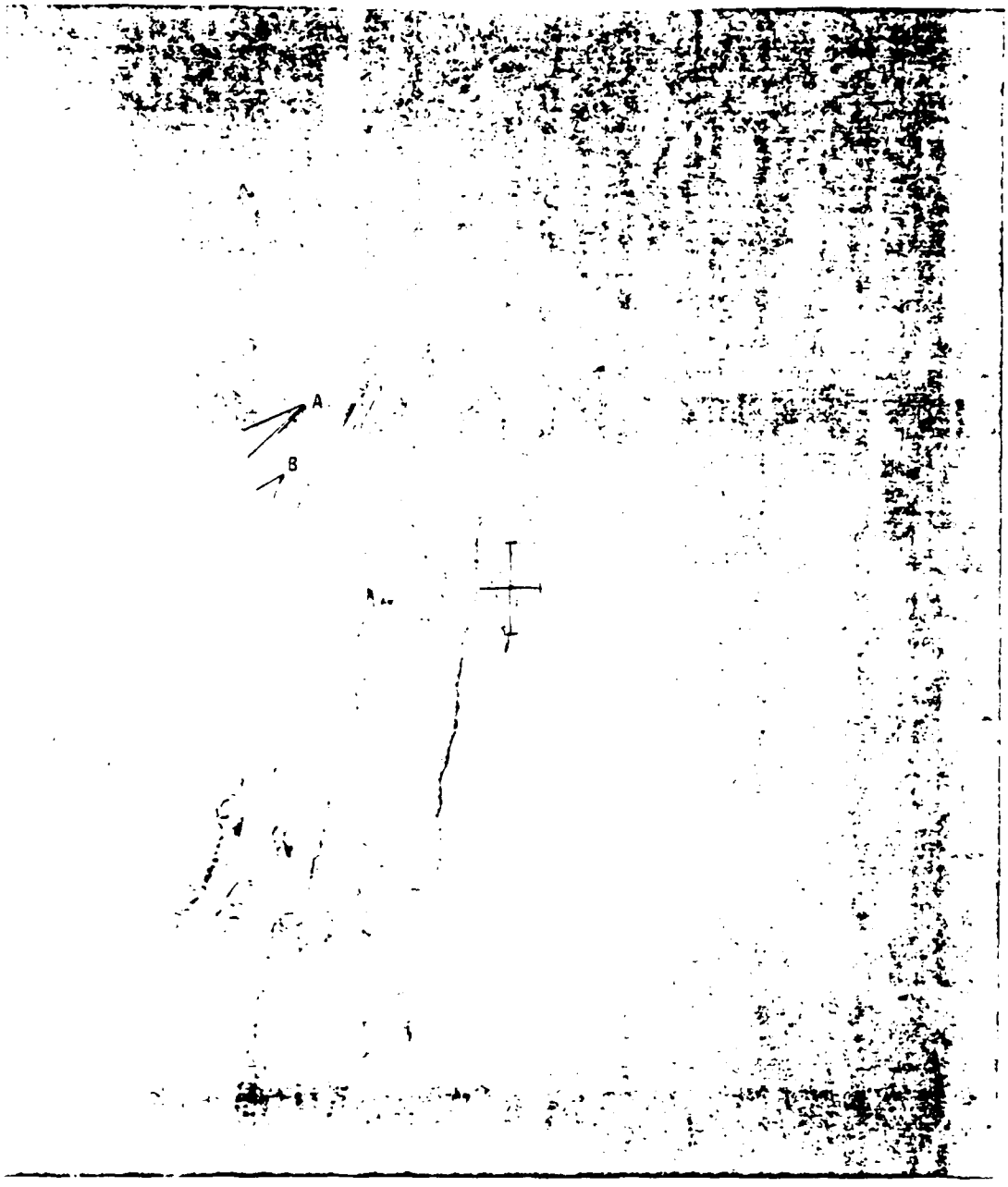

Figure 31. Photograph 61-A 200 45

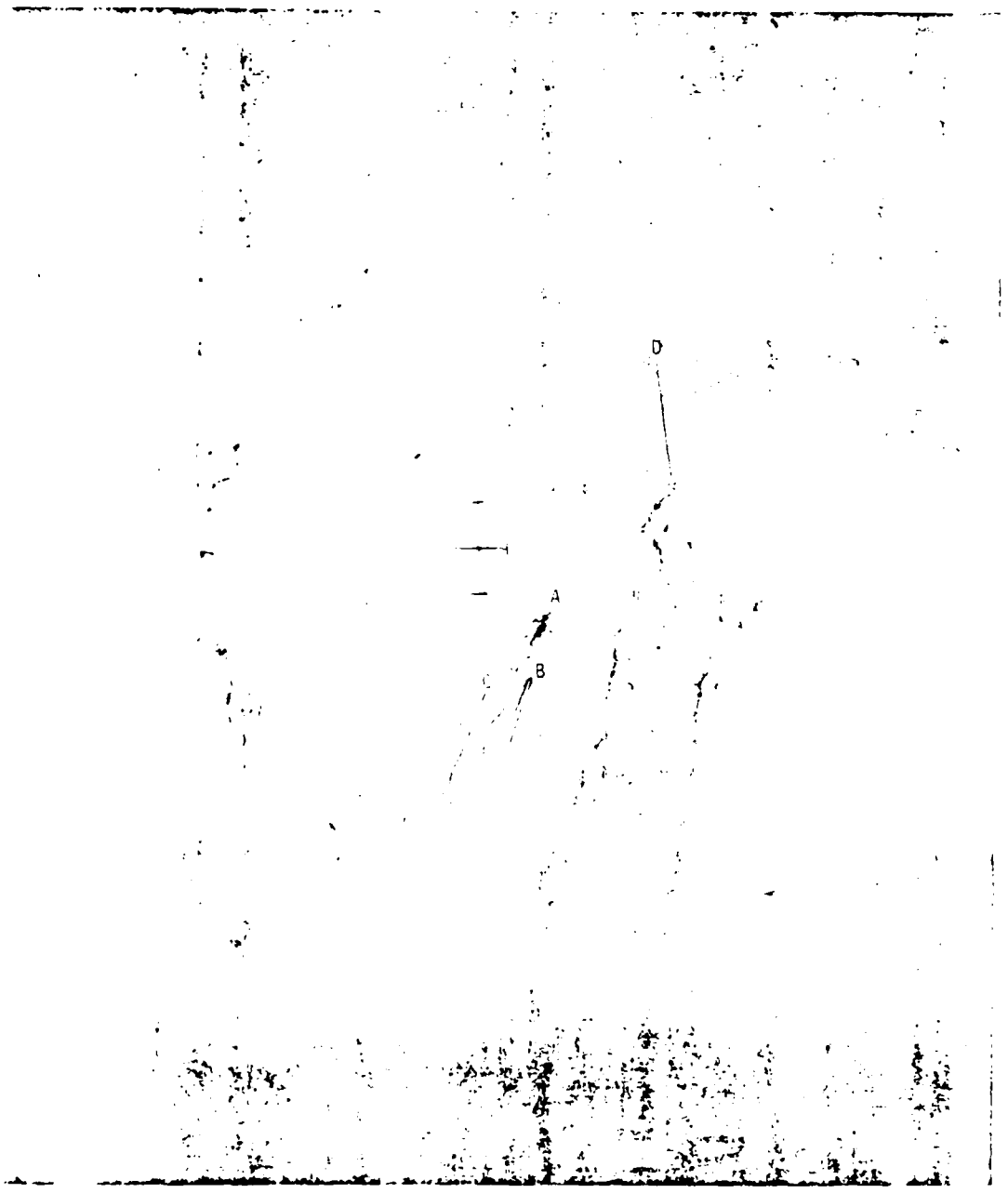

Figure 32. Photograph 61-A 200 46

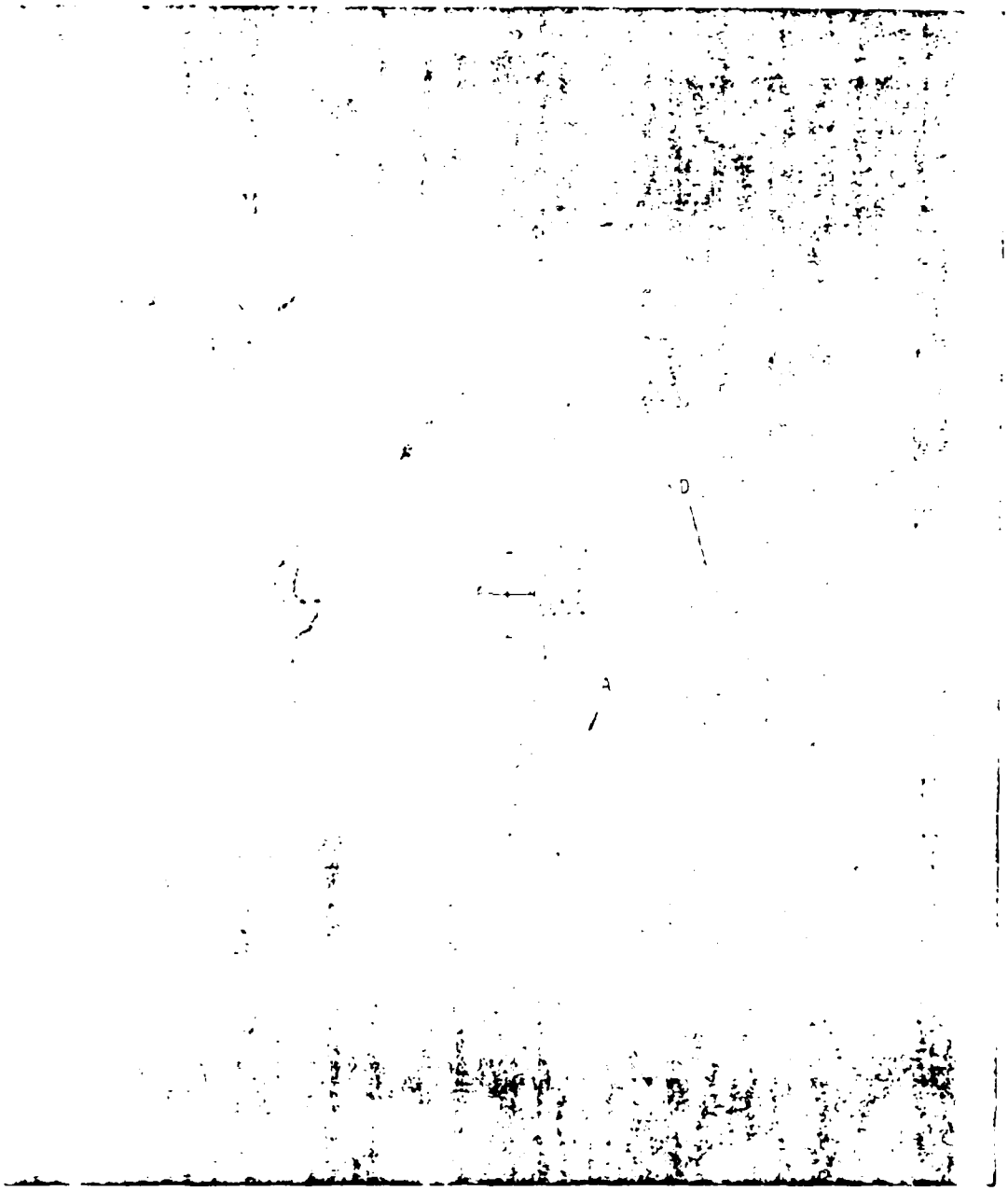

Figure 33. Photograph 61-A 200 47

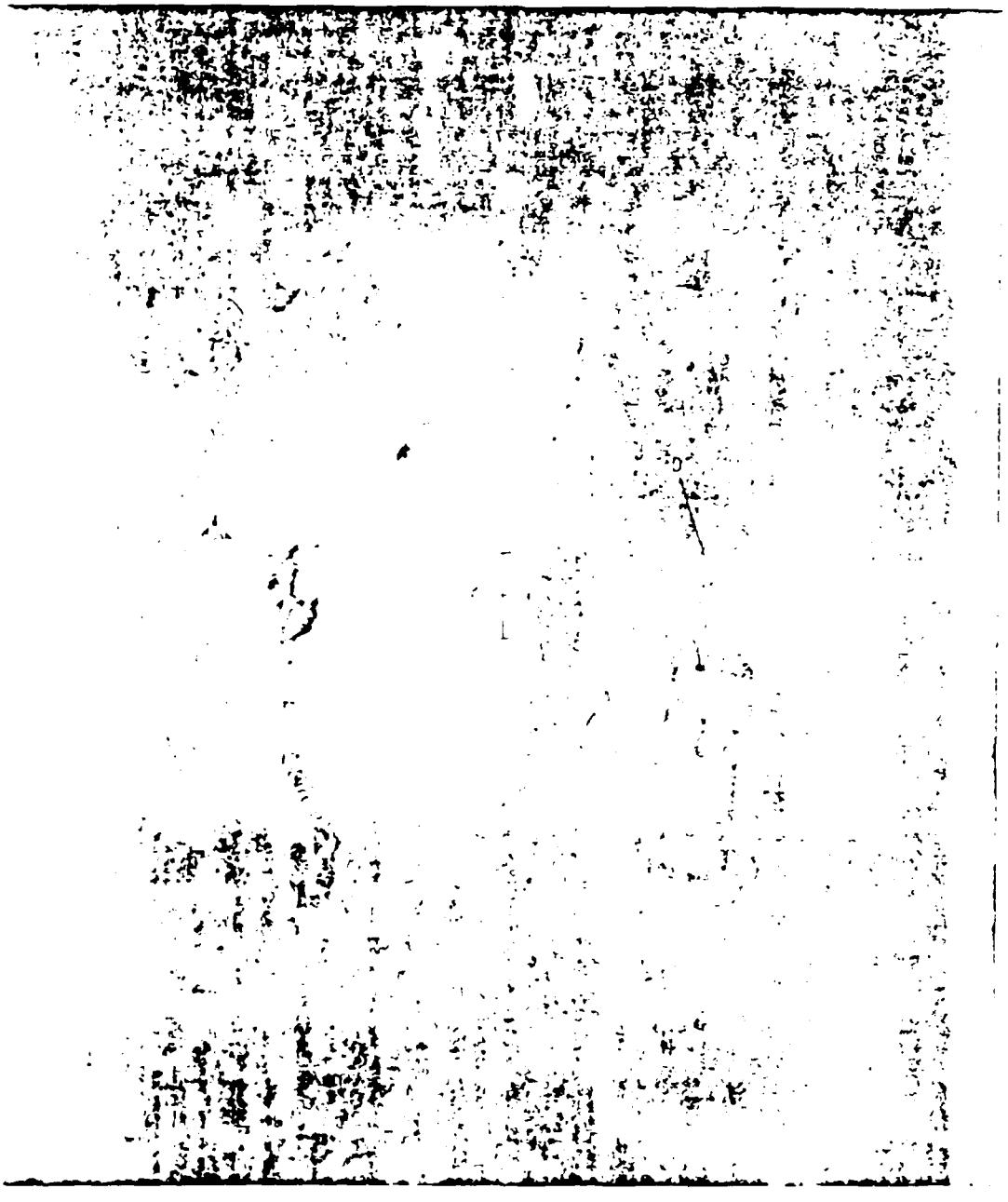

Figure 34 Photograph 61-A-200-48

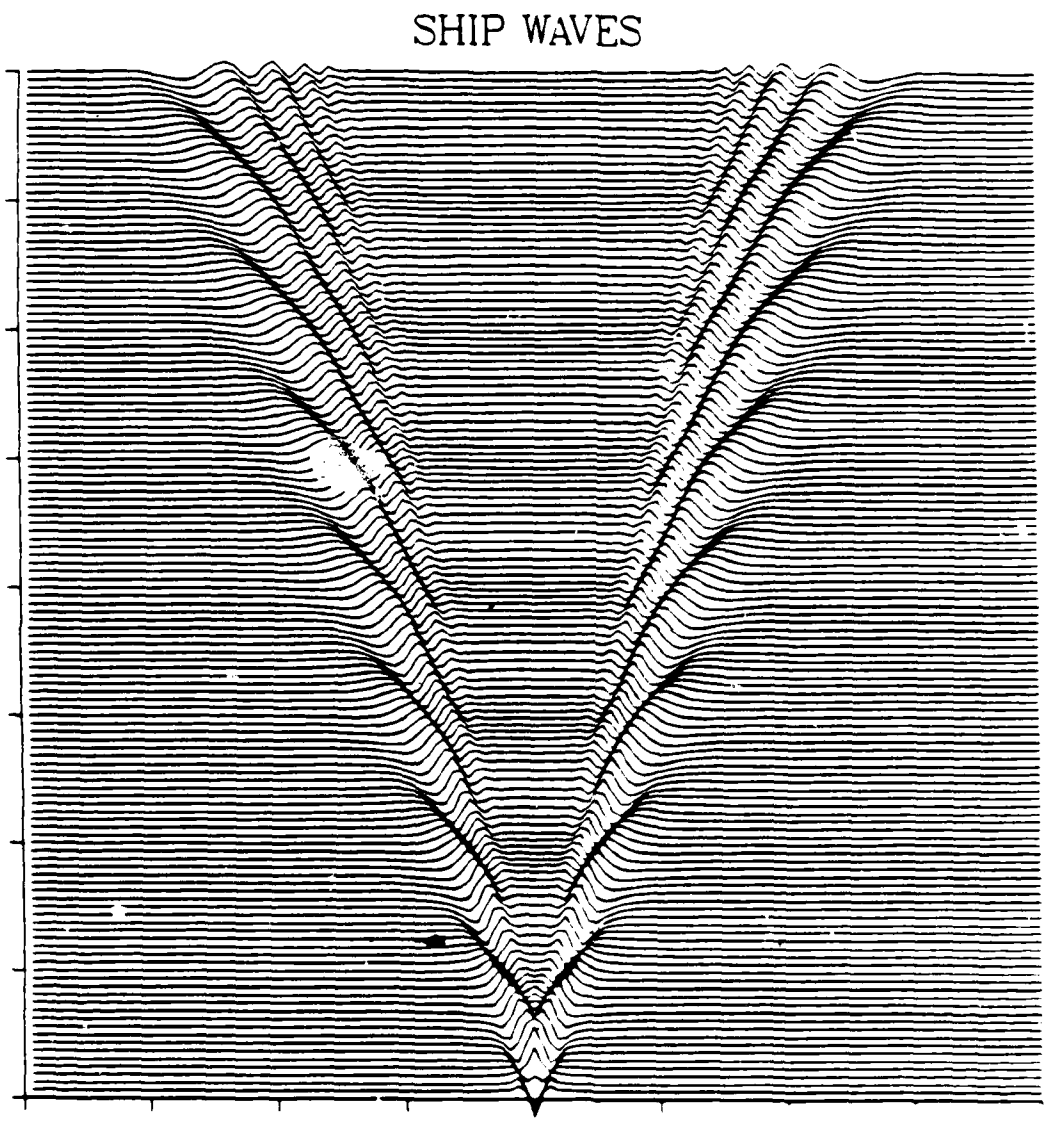

Figure 35. Kelvin wave elevations for an idealized ship at the surface

SHIP WAVES

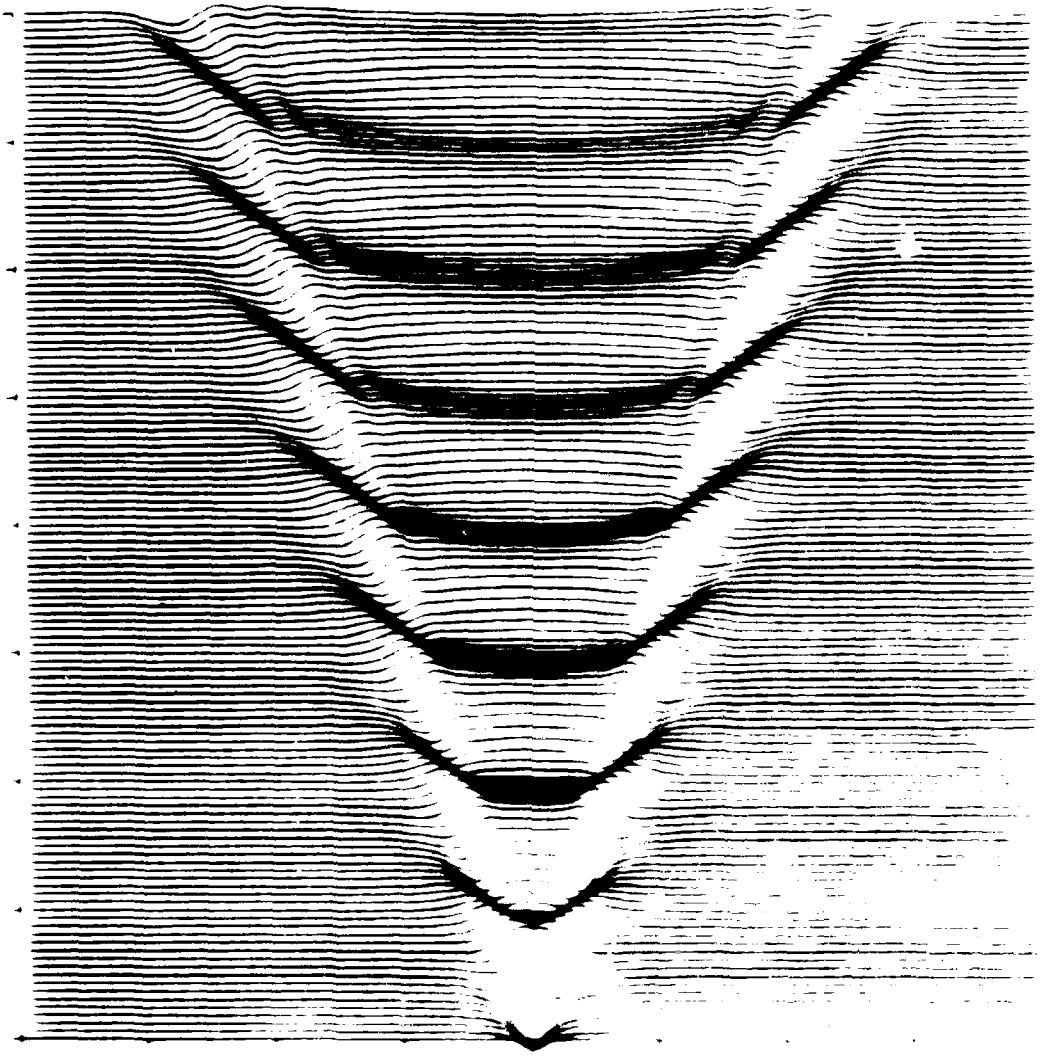

Figure 10. [illegible]

SHIP WAVES

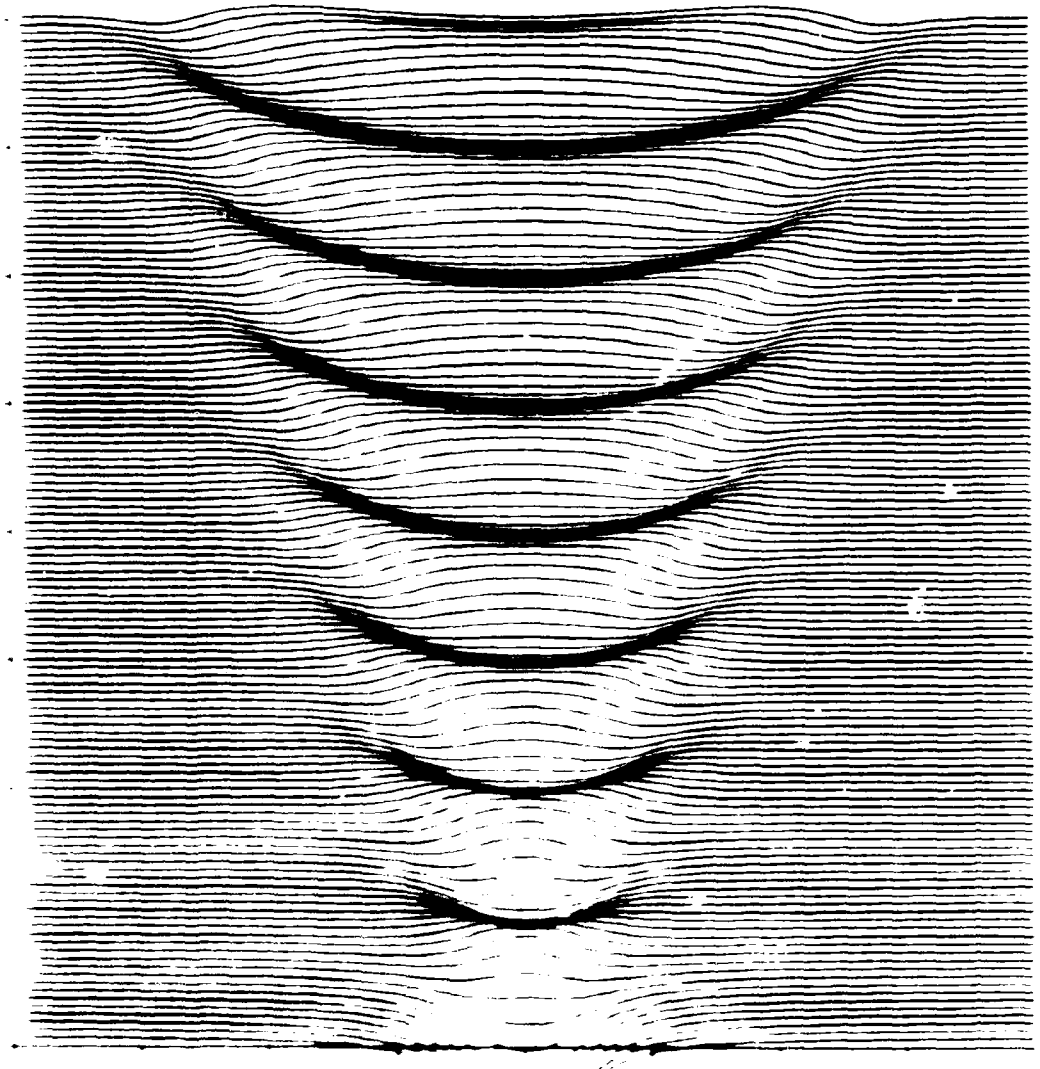

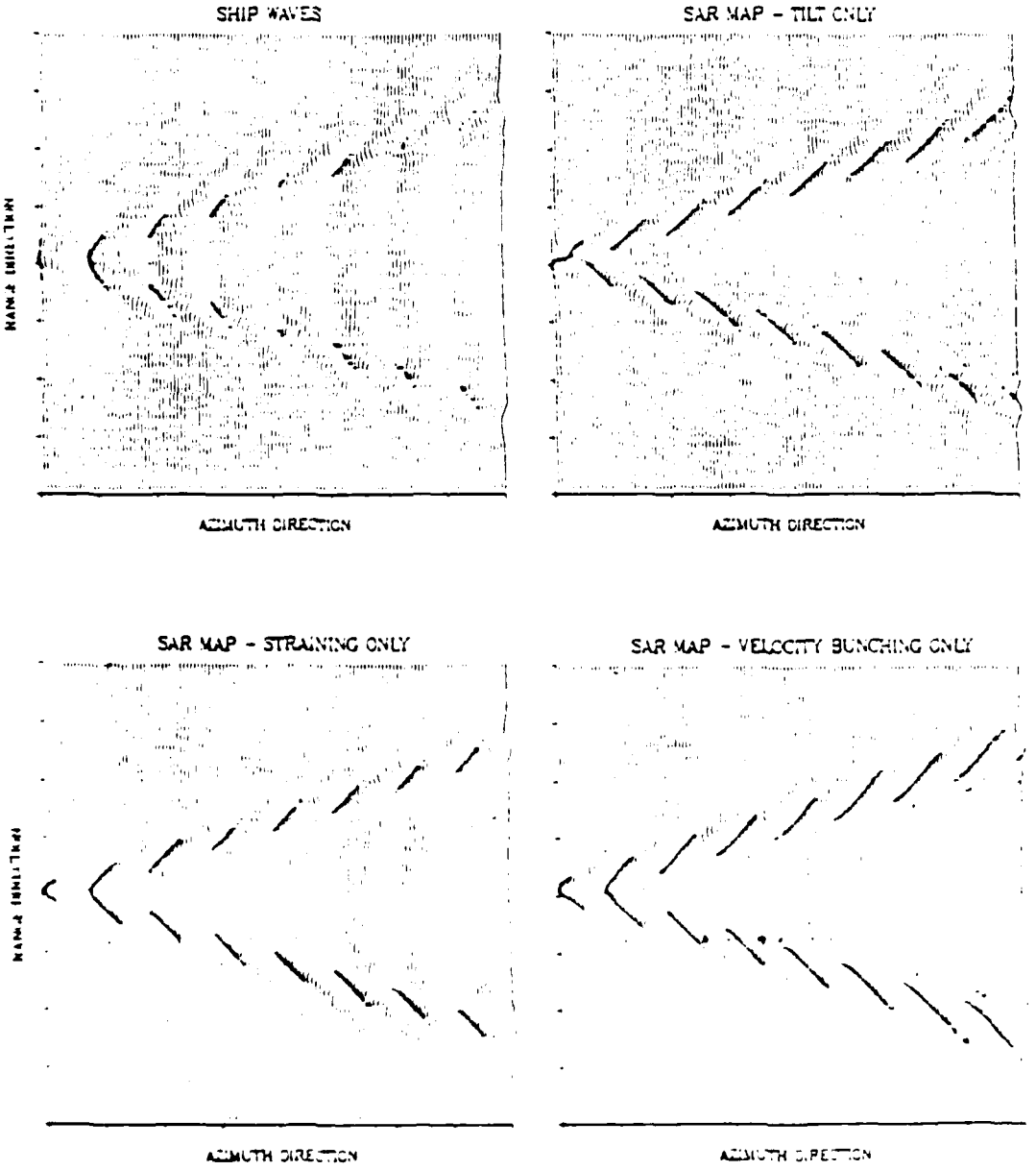

Figure 38 Synthetic aperture radar imaging of waves from an azimuthally traveling ship by the three principal mechanisms: tilt, straining, and velocity bunching

END

9-87

DTIC